Chapter 6

MICROMECHANICS

In this chapter, we examine a variety of means of calculating elastic and physical properties of metal matrix composites, given the same constants for the individual components and the arrangement of components in the composite; and thermal stresses generated because of mismatch in the coefficient of thermal expansion (CTE) of the components. In fact, most of the material discussed in this chapter is applicable to all kind of composites. Specifically, we provide a micromechanical description of physical properties such as density, thermal expansion coefficients, thermal and electrical conductivity, and various elastic constants. Of particular interest are methods or expressions that predict elastic constants of composites because of the generally high anisotropy found in composites. A description of conventional and microstructure-based finite element techniques to predict the elastic and thermal constants is also provided.

We briefly review the theory of elasticity and the concept of number of independent elastic constants required for a fiber reinforced composite. We then provide expressions for the elastic constants as per different schemes available. This is followed by a description of physical properties and thermal stresses in composites.

6.1 ELASTIC CONSTANTS OF A FIBER REINFORCED COMPOSITE

Hooke's law relates the second rank **stress** tensor, σ_{ij}, and the second rank **strain** tensor, $\varepsilon_{k\ell}$, and can be written as:

$$\sigma_{ij} = C_{ijkl}\varepsilon_{k\ell} \tag{6.1}$$

where C_{ijkl} is a fourth-rank tensor called the elastic stiffness tensor and the indices i, j, k, and ℓ have values of 1, 2, and 3. The stress and strain tensors, being second rank, have $3^2 = 9$ components each. The stiffness tensor is a fourth rank tensor, it has $3^4 = 81$ components. Stress, strain, and stiffness are symmetric tensors, i.e., $\sigma_{ij} = \sigma_{ji}$, $\varepsilon_{k\ell} = \varepsilon_{\ell k}$, and $C_{ijk\ell} = C_{k\ell ji} = C_{ji\ell k} = C_{jik\ell}$. These symmetry relationships reduce the maximum number of independent elastic constants to 21. Hooke's law in (Eq. 6.1) can then be simplified and rewritten in a contracted notation more appropriate for matrix operations as follows:

$$\sigma_i = C_{ij}\varepsilon_j \qquad (6.2)$$

In a similar manner we can write Hooke's law in terms of the elastic compliance matrix, S_{ij}, as:

$$\varepsilon_i = S_{ij}\sigma_j \qquad (6.3)$$

Both C_{ij} and S_{ij} are 6 x 6 symmetric matrices, i.e., $C_{ij} = C_{ji}$ and $S_{ij} = S_{ji}$. Also, the stiffness and the compliance matrices are inverse of each other, i.e.:

$$[C][S] = [I]$$

where $[I]$ is the identity matrix. The total number of independent constants required to describe the elastic behavior of a material completely decreases with increasing symmetry elements present. Table 6.1 presents a summary.

Table 6.1: Independent elastic constants for systems of different symmetry.

Symmetry	**Number of Independent Constants**	**Constants**
Orthorhombic	9	$C_{11}, C_{12}, C_{13}, C_{22}, C_{23}, C_{33}, C_{44}, C_{55}, C_{66}$
Trigonal	6	$C_{11}, C_{12}, C_{13}, C_{14}, C_{33}, C_{44}$
Tetragonal	6	$C_{11}, C_{12}, C_{13}, C_{33}, C_{44}, C_{66}$
Hexagonal	5	$C_{11}, C_{12}, C_{13}, C_{33}, C_{44}$
Cubic	3	C_{11}, C_{12}, C_{44}
Isotropic	2	C_{11}, C_{12}

For an isotropic material, there are only two independent elastic constants. For a material with cubic symmetry, we need three independent elastic constants. The most general situation is that of the triclinic system (not shown in Table 6.1) in which there are no symmetry elements present; it requires 21 independent elastic constants. For a material with cubic symmetry, we can write Hooke's law in an extended form as follows:

$$\begin{bmatrix} \sigma_1 \\ \sigma_2 \\ \sigma_3 \\ \sigma_4 \\ \sigma_5 \\ \sigma_6 \end{bmatrix} = \begin{bmatrix} C_{11} & C_{12} & C_{12} & 0 & 0 & 0 \\ & C_{11} & C_{12} & 0 & 0 & 0 \\ & & C_{11} & 0 & 0 & 0 \\ & & & C_{44} & 0 & 0 \\ & & & & C_{44} & 0 \\ & & & & & C_{44} \end{bmatrix} \begin{bmatrix} \varepsilon_1 \\ \varepsilon_2 \\ \varepsilon_3 \\ \varepsilon_4 \\ \varepsilon_5 \\ \varepsilon_6 \end{bmatrix}$$

Note that there are only three independent constants. For an isotropic material, the number of independent constants is reduced from 3 to 2 because of the following relationship:

$$C_{11} - C_{22} = 2C_{44}$$

In engineering usage, for an isotropic material, any two of the following four constants will suffice: Young's modulus (E), Poisson's ratio (ν), shear modulus (G), and bulk modulus (K). This is because of the following relationships among the four constants:

$$E = 3K(1 - 2\nu)$$

$$G = \frac{E}{2(1+\nu)}$$

$$K = \frac{E}{3(1-2\nu)}$$

$$\text{and } \nu = \frac{E}{2G} - 1$$

Thus, only two of the four constants for an isotropic material are independent.

A unidirectionally reinforced fiber reinforced composite with fibers arranged in a random manner in the transverse section is said to be transversely isotropic, i.e., there is no preferred direction in the 2-3 plane, see Fig. 6.1. Such an arrangement of fibers gives us the same elements as the hexagonal crystal, i.e., five independent elastic constants are needed to fully describe the elastic behavior of such a composite. Note that this follows from the disposition of long fibers in a matrix, even though the two components, fiber and matrix, may individually be isotropic in nature. On the other hand, a particle or whisker/short fiber reinforced composite, with no preferential alignment of reinforcement, can be treated as an isotropic material. We describe a variety of approaches to obtain the elastic constants of the composite below, given the elastic constants of the individual components.

6.1.1 Strength of Materials Approach

We can get some quick estimates of elastic constants of a composite by using the strength of materials approach. Here we make simplifying assumptions of uniform strain or uniform stress in the constituents of the composite. The results are satisfactory for E_{11} and ν_{12}, but underestimate E_{22} and G_{12}. We use $E_{c\ell}$ and E_{11} interchangeably to indicate longitudinal Young's modulus in the fiber direction. Similarly, E_{ct} and E_{22} indicate Young's modulus in the direction transverse to the fiber axis. Two simple

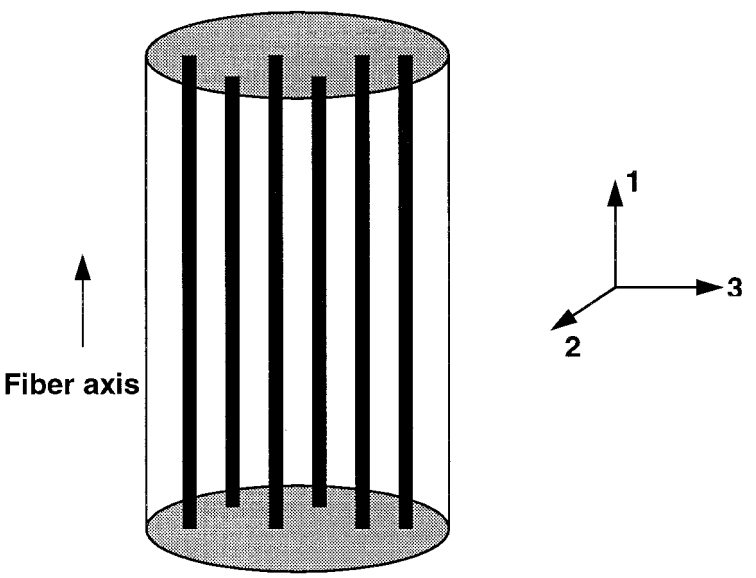

Fig. 6.1 A unidirectionally reinforced fiber reinforced composite with fibers arranged in a random in the transverse (2-3) plane. Such a composite is called transversely isotropic.

cases are *isostrain* and *isostress* models for Young's modulus of a unidirectionally aligned, fiber reinforced composite, see Fig. 6.2. We shall also derive expressions for the principal shear modulus and principal Poisson's ratio.

Longitudinal Young's Modulus

If we apply the *isostrain* condition to a unidirectional, fiber reinforced composite loaded along the fiber direction, we get the longitudinal Young's modulus, E_{cl} or E_{11}, of the composite. The isostrain condition says that the strains in the fiber, matrix, and composite are identical, see Fig. 6.2; i.e.:

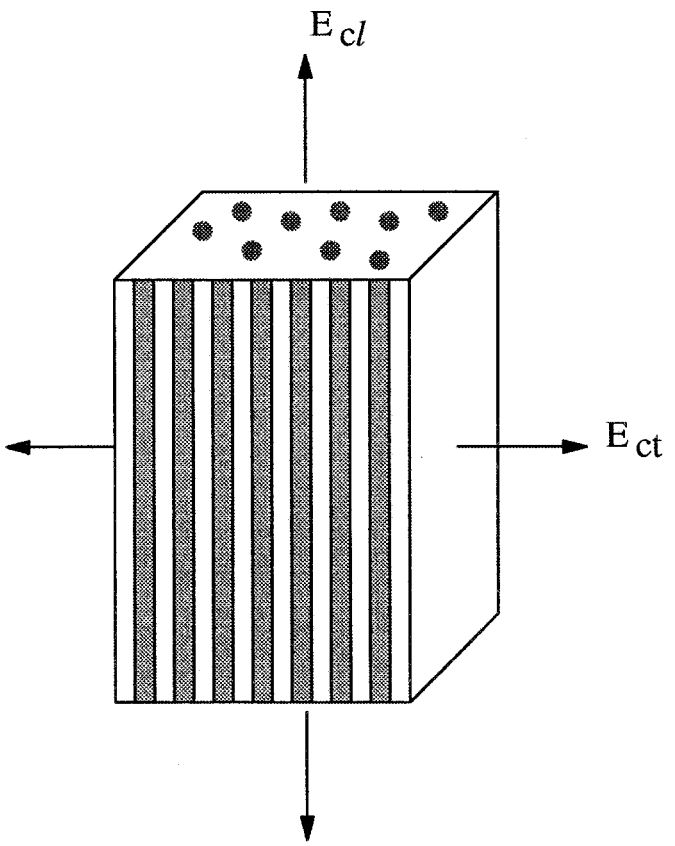

Fig. 6.2 Longitudinal ($E_{c\ell}$) and transverse (E_{ct}) Young's moduli for a unidirectionally reinforced fiber reinforced composite.

$$\varepsilon_f = \varepsilon_m = \varepsilon_{c\ell} = \frac{\Delta \ell}{\ell_o} \qquad (6.4)$$

where ε is the strain, $\Delta\ell$ is the change in length, ℓ_o is the original length, and the subscripts f, m, and cℓ indicate fiber, matrix, and composite in the longitudinal direction, respectively.

For components behaving elastically, we can use Hooke's law for a uniaxial stress acting on the fiber and the matrix:

$$\sigma_f = E_f \varepsilon_{c\ell} \quad \text{and} \quad \sigma_m = E_m \varepsilon_{c\ell}$$

where σ is the stress, E is the Young's modulus, and the subscripts have the meanings given above.

The applied load on the composite, P_c, is partitioned between the fiber and the matrix, i.e.:

$$P_c = P_f + P_m$$

where P_f and P_m indicate the load on the fiber and matrix, respectively. Converting loads into stresses, we can write:

$$\begin{aligned}
\sigma_{c\ell} A_c &= \sigma_f A_f + \sigma_m A_m \\
&= E_f A_f \varepsilon_{c\ell} + E_m A_m \varepsilon_{c\ell} \\
&= (E_f A_f + E_m A_m)\, \varepsilon_{c\ell} \\
\sigma_{c\ell} &= E_{c\ell} \varepsilon_{c\ell} = (E_f A_f + E_m A_m)\, \varepsilon_{c\ell}
\end{aligned}$$

From this we get the following expressions:

$$E_{c\ell} = E_f V_f + E_m V_m \qquad (6.5)$$

$$\sigma_{c\ell} = E_{c\ell} \varepsilon_{c\ell} = (E_f A_f + E_m A_m)\, \varepsilon_{c\ell} \qquad (6.6)$$

It turns out that predictions given by Eq. 6.5 are quite reasonable. As an example, Fig. 6.3 shows the linear dependence of longitudinal Young's modulus of a tungsten fiber reinforced copper as a function of fiber volume fraction (McDanels et al., 1965).

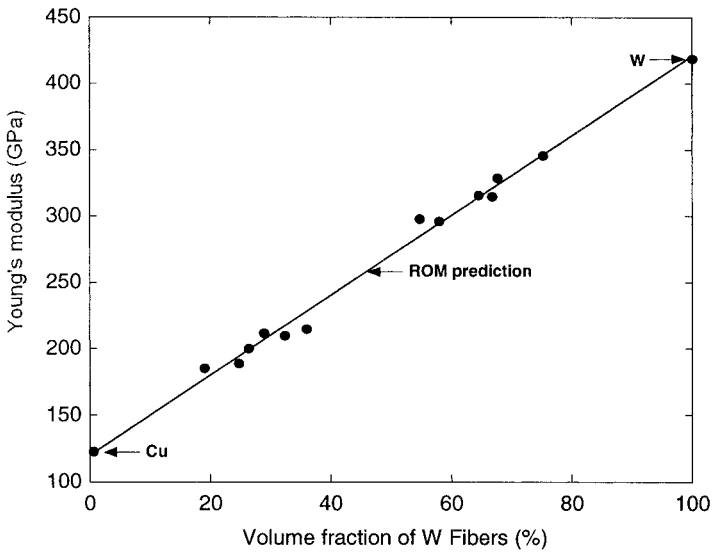

Fig. 6.3 Linear dependence of longitudinal Young's modulus of tungsten fiber reinforced copper as a function of fiber volume fraction (after McDanels et al., 1965).

Transverse Young's Modulus

The transverse modulus, E_{ct} or E_{22}, can be estimated by applying an isostress condition, i.e., the fiber, matrix, and composite experience the same stress, Fig. 6.2. Thus:

$$\sigma_f = \sigma_m = \sigma_{ct} \tag{6.7}$$

where the subscript ct denotes the composite in the transverse direction, and the other subscripts have the significance given earlier.

The total displacement of the composite in the thickness direction, Δt_c, is the sum of the displacement in the fiber, Δt_f, and that in the matrix, Δt_m. We can then write the following relationship for the displacement in the thickness direction:

$$\Delta t_c = \Delta t_m + \Delta t_f$$

Let the original thickness of the composite be t_c. Dividing throughout by t_c, the gage length, we get the strain in the transverse direction:

$$\varepsilon_{ct} = \frac{\Delta t_c}{t_c} = \frac{\Delta t_m}{t_m}\frac{t_m}{t_c} + \frac{\Delta t_f}{t_f}\frac{t_f}{t_c}$$

$$\varepsilon_{ct} = \varepsilon_m \frac{\Delta t_m}{t_c} + \varepsilon_f \frac{t_f}{t_c} \qquad (6.8)$$

Also, we can write the volume fractions of fiber and matrix as:

$$V_m = \frac{t_m}{t_c} \quad \text{and} \quad V_f = \frac{t_f}{t_c}$$

Using Hooke's Law, we can rewrite Eq. (6.8) as:

$$\frac{\sigma_{ct}}{E_{ct}} = \frac{\sigma_{ct} V_m}{E_m} + \frac{\sigma_{ct} V_f}{E_{ft}}$$

or

$$\frac{1}{E_{ct}} = \frac{V_m}{E_m} + \frac{V_f}{E_{ft}} \qquad (6.9)$$

We should point out that when computing Young's modulus in the transverse direction, we have chosen the transverse modulus of the fiber, E_{ft}. This is especially important when the fiber is anisotropic, for example, carbon fiber.

Poisson's Ratio

Consider a composite containing unidirectionally aligned fibers loaded in tension parallel to the fibers, see Fig. 6.4. The composite will extend longitudinally by ε_1 (direction 1) and contract transversely by ε_2 (direction 2). The contraction in direction 2 due to all the fibers will be $-\varepsilon_1 V_f \nu_f$, where V_f is the fiber volume fraction and ν_f is the Poisson's ratio of the fiber. The contraction due to the matrix will be $-\varepsilon_1 V_m \nu_m$, where V_m is the matrix volume fraction and ν_m is the Poisson's ratio of the matrix.

The total contraction of the composite in direction 2 is then given by:

$$\varepsilon_2 = -\varepsilon_1 V_f \nu_f - \varepsilon_1 V_m \nu_m$$

$$= -\varepsilon_1 (V_f \nu_f + \varepsilon_1 V_m \nu_m)$$

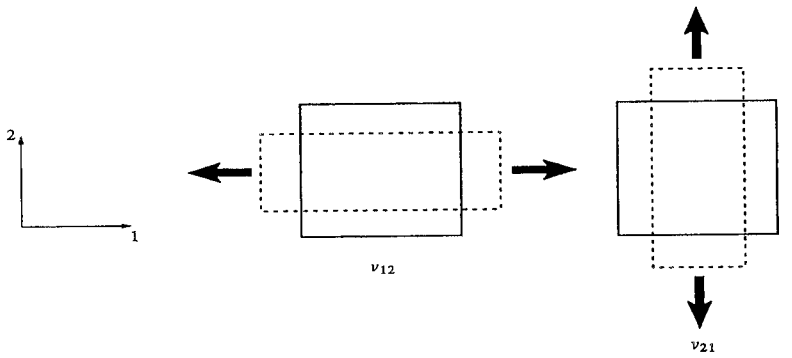

Fig. 6.4 The two Poisson's ratios in an anisotropic material. The principal Poisson's ratio (ν_{12}) gives the transverse strain caused by an axial stress. The secondary Poisson's ratio (ν_{21}) gives the axial strain caused by a transversely applied stress.

Defining the principal Poisson's ratio of the composite as $\nu_{12} = -\varepsilon_2/\varepsilon_1$ we get:

$$\nu_{12} = V_f \nu_f + V_m \nu_m$$

Shear Modulus

In the case of longitudinal or principal shear modulus, both the fiber and matrix are subjected to the same shear stress as shown in Fig. 6.5. Note that the fibers have been bundled together to show total shear in all the fibers. We can write the shear strain in the matrix and fiber as follows:

$$\gamma_m = \frac{\tau_m}{G_m}$$

and

$$\gamma_f = \frac{\tau_f}{G_f}$$

The total shear displacement in the composite, Δ, is given by:

$$\Delta = \gamma t$$

where γ is the average shear strain in the composite and t is the thickness of the composite. We can then write the total shear displacement as the sum of the shear displacements of the components:

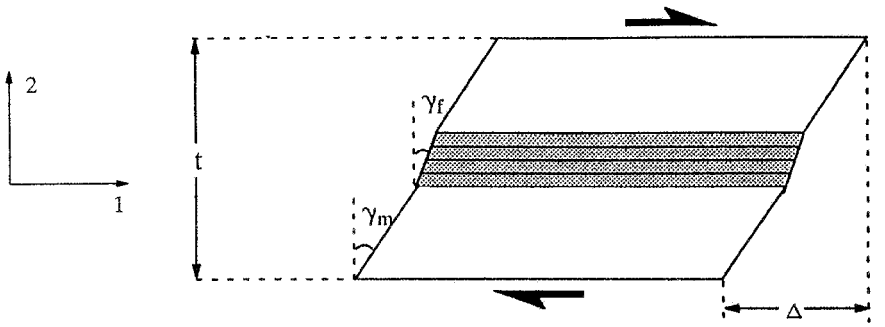

Fig. 6.5 A unidirectional fiber reinforced composite loaded in shear parallel to the fibers.

$$\Delta = \Delta_f + \Delta_m$$

or,

$$\Delta = \gamma_f V_f t_f + \gamma_m V_m t_m$$

$$\gamma = \frac{\Delta}{t} = \gamma_f V_f + \gamma_m V_m$$

Shear strain, γ, is nothing but shear stress divided by shear modulus, G_{12}, i.e.,:

$$\tau/G_{12} = V_m \tau/G_m + V_f \tau/G_f$$

or $$1/G_{12} = V_m/G_m + V_f/G_f$$

6.1.2 Micromechanical Approaches

In this section we include the following important techniques:

- Self-consistent field methods
- Variational calculus methods
- Numerical methods

Brief descriptions of these as well as some key results are presented below.

Self-Consistent Field Methods: The strength of materials approach described above involves gross simplification of uniform stress (isostress) or

uniform strain (isostrain). Self-Consistent (SC) models improve on the internal stress and strain fields by introducing a simplified geometry of the phases. It should be pointed out, though, that in these techniques one still makes approximations of microstructure, i.e., the actual microstructure is not used. In one version, the phase geometry is represented by one single fiber embedded in a matrix cylinder. This outer cylinder is embedded in an infinite, homogeneous material whose properties are taken to be the average properties of the composite. In the second version, a three-cylinder model is used. The intermediate cylinder surrounding the fiber has the properties of the matrix. The outermost cylinder has average properties of the composite. The radii of the cylinders are dictated by the fiber volume fraction. A uniform load, applied at infinity, introduces a uniform strain field in the fiber. Elastic constants are then obtained from this strain field. The results obtained are independent of fiber arrangements in the matrix and, in general, are reliable at low fiber volume fractions (V_f), reasonable at intermediate V_f, and unreliable at high V_f (Hill, 1964).

Variational Calculus or Energy Methods: Energy methods involving variational calculus can be used to obtain bounds on a property of the composite. These techniques are also called bounding methods. Effective elastic constants (or compliances) of a composite (a heterogeneous system) are obtained from those of a homogeneous system with the same free energy. In simple terms, we can describe the rationale behind these methods as follows. Consider a linear elastic solid under deformation. We can express the strain energy stored in this solid in terms of a strain field:

$$U_s = \frac{1}{2} S_{ij} \sigma_j$$

and in terms of stress field:

$$U_c = \frac{1}{2} C_{ij} \varepsilon_j$$

These two expressions are equivalent for a homogeneous material but not for a heterogeneous material. The difference between these two expressions for a heterogeneous material (i.e., a composite) can be exploited to obtain the upper and lower bounds. Specifically, the theorem of least work gives the lower bound while the theorem of minimum potential energy provides the upper bound. There is a considerable amount of literature available on the subject; see, for example, Paul (1960); Hermans (1967); Hashin and Rosen (1964); Whitney and Riley (1966).

These bounding methods do not predict properties exactly, but give upper and lower bounds on elastic constants. The property is determined exactly only if the upper and lower bounds coincide. More often than not, the upper and lower bounds are not very close. Only when these bounds are close enough can we safely use them as indicators of the material behavior. It turns out that this is the case for longitudinal properties of a unidirectionally aligned fiber reinforced composite such as longitudinal constants (E_{11}, ν_{12}), but they can be far apart in case of transverse and shear properties (E_{22} and G_{12}).

Hill (1965) derived bounds for the elastic constants. In particular, he put rigorous bounds on the longitudinal Young's modulus, E, in terms of bulk modulus in plane strain (k_p), Poisson's ratio (ν), and the shear modulus (G) of the two phases. No restrictions were made on fiber form or packing geometry. The bulk modulus in plane strain, k_p, is the modulus for lateral dilation with zero longitudinal strain and is given by:

$$k_p = \frac{E}{2(1-2\nu)(1+\nu)}$$

The bounds on the longitudinal modulus, $E_{c\ell}$, are:

$$4V_fV_m(\nu_f-\nu_m)^2 / (V_f/k_{pm} + V_m/k_{pf} + 1/G_m)$$

$$\leq E_{c\ell} - E_fV_f - E_mV_m \leq$$

$$4V_fV_m(\nu_f-\nu_m)^2 / (V_f/k_{pm} + V_m/k_{pf} + 1/G_f) \qquad (6.10)$$

We can readily verify, from Eq. 6.10, that deviations from the rule of mixtures for $E_{c\ell}$ are quite small. If we substitute some values of practical composites, such as silicon carbide fibers in an aluminum matrix, we find that the deviations in $E_{c\ell}$ from the rule of mixtures are < 2%. Note that the deviation from the rule-of-mixtures value comes in from the $(\nu_f - \nu_m)^2$ factor. For $\nu_f = \nu_m$, we have $E_{c\ell}$ given precisely by the rule-of-mixtures expression. Numerical simulations confirm that Hill's bounds are the best possible general bounds for linear elastic behavior of unidirectionally aligned fiber reinforced composites under axial loading (Rossoll et al., 2005)

For Poisson's ratio of a unidirectionally aligned fiber composite, Hill also showed that

$$\nu_{12} > \nu_fV_f + \nu_mV_m \text{ for } (\nu_f-\nu_m)(k_{pf}-k_{pm}) > 0,$$

$$\text{and} \quad \nu_{12} < \nu_f V_f + \nu_m V_m \text{ for } (\nu_f - \nu_m)(k_{pf} - k_{pm}) < 0 \qquad (6.11)$$

If $\nu_f < \nu_m$ and $E_f >> E_m$, then, ν_{12} will be less than that predicted by the rule of mixtures ($= \nu_f V_f + \nu_m V_m$). It is easy to see that the bounds on ν_{12} are not as close as the ones on $E_{c\ell}$. This is because $(\nu_f - \nu_m)$ appears in the case of ν_{12} (Eq. 6.13), while $(\nu_f - \nu_m)^2$ appears in the case of $E_{c\ell}$ (Eq. 6.10). If $(\nu_f - \nu_m)$ is very small, the bounds will be close enough to allow us to write:

$$\nu_{12} \approx \nu_f V_f + \nu_m V_m \qquad (6.12)$$

We can summarize the results of Hashin and Rosen (1964) and Hill (1965) as follows. For a transversely isotropic composite, with fibers along direction 1 and the 2-3 plane being the transverse (isotropic) plane, the equations for five independent moduli are given below.

Plane-strain bulk modulus, k_{23}:

$$k_{23} = \frac{k_f k_m + G_m(\nu_f k_f + \nu_m k_m)}{G_f + \nu_m k_f + \nu_f k_m}$$

where k_m and k_f are the plane-strain bulk moduli of the matrix and fiber, respectively. The plain-strain bulk modulus is defined as:

$$k = K + \frac{1}{3}G$$

In-plane shear modulus, G_{12}:

$$G_{12} = G_m \frac{G_f(1+V_f) + G_m V_m}{G_f V_m + G_m(1+V_f)}$$

Longitudinal Young's modulus, E_{11}:

$$E_{11} = E_f V_f + E_m V_m + \left[4V_f V_m(\nu_m - \nu_f)^2\right] / \left[(V_f / k_m) + (V_m / k_f) + 1/G_m\right]$$

For most practical purposes the last term is negligible in the above expression.

Longitudinal Poisson's ratio, ν_{12}:

$$\nu_{12} = \nu_f V_f + \nu_m V_m + [V_f V_m (\nu_f - \nu_m)][(1/k_m) - (1/k_f)/(V_f/k_m) + (V_m/k_f) + 1/G_m]$$

Transverse plane shear modulus, G_{23}:

In this case, the upper and lower bounds are not coincident. The lower bound is:

$$G_{23L} = G_m + \frac{V_f}{\frac{1}{G_f - G_m} + (K_m + 2G_m)\frac{V_m}{2G_m(k_m + G_m)}}$$

The upper bound is:

$$G_{23U} = G_m + \frac{(\alpha + \beta_m V_f)(1 + \rho\nu_f^3) - 3\nu_f \nu_m^2 \beta_m^2}{(\alpha - \nu_f)(1 + \rho\nu_f^3) - 3\nu_f \nu_m^2 \beta_m^2}$$

where

$$\alpha = \frac{\gamma + \beta_m}{\gamma - 1} \qquad \rho = \frac{\beta_m - \gamma\beta_f}{1 + \gamma\beta_f}$$

$$\gamma = \frac{G_f}{G_m} \qquad \beta_m = \frac{1}{3 - 4V_m} \qquad \beta_f = \frac{1}{3 - 4V_f}$$

For particulate composites, Hashin (1962) proposed a composite sphere assembly model wherein the composite is made up of units consisting of a spherical particle and its surrounding matrix shell. In each spherical unit, the volume fractions of the particle and matrix are the same, but the spherical units can be of any size. Figure 6.6 shows such an assembly. Hashin analyzed this model by variational calculus methods and obtained a closed-form solution for the bulk modulus and upper and lower bounds for the effective shear modulus. The bulk modulus, K, is given by:

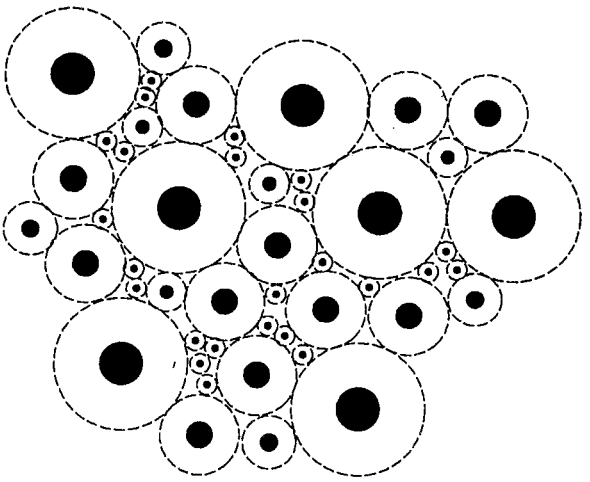

Fig. 6.6 A composite made up of an assemblage of spherical particles surrounded by their respective matrix shells. The volume fractions of phases are maintained constant in each unit; individual units can be of any size.

$$K = \frac{K_p K_m + \frac{4}{3} G_m (V_p K_p + V_m K_m)}{V_p K_m + V_m K_p + \frac{4}{3} G_m}$$

where K, G, and V indicate the bulk modulus, shear modulus, and volume fraction, respectively, and the subscripts p and m refer to the particle and the matrix, respectively. Hashin and Shtrikman (1963) and Rosen (1973) have also analyzed macroscopically isotropic, particulate composite with an arbitrary internal phase geometry and only phase volume fractions being specified. The bounds of Hashin and Shtrikman on the bulk modulus, K and shear modulus, G are given below:

$$K_{upper} = K_p + (1 - V_p)\left[\frac{1}{K_m - K_p} + \frac{3V_p}{3K_p + 4G_p}\right]^{-1}$$

$$K_{lower} = K_m + V_p\left[\frac{1}{K_p - K_m} + \frac{3(1 - V_p)}{3K_m + 4G_m}\right]^{-1}$$

$$G_{upper} = G_p + (1 - V_p)\left[\frac{1}{G_m - G_p} + \frac{6V_p(K_p + 2G_p)}{5G_p(3K_p + 4G_p)}\right]^{-1}$$

$$G_{lower} = G_m + V_p\left[\frac{1}{G_p - G_m} + \frac{6(1 - V_p)(K_m + 2G_m)}{5G_m(3K_m + 4G_m)}\right]^{-1}$$

where $K_m > K_p$ and $G_p > G_m$. For $K_m < K_p$ and $G_p < G_m$ the inequalities will be reversed. Treating the particulate composite as an isotropic material, we can obtain the bounds on the Young's modulus of the composite, E_c, by using the following relationship:

$$E = \frac{9K}{1+3K/G}$$

We can easily use this relationship to obtain the bounds on Young's modulus. For $0.5 < E_p/E_m < 3$, the bounds are close enough to give us a value within ~10 % of the true modulus.

6.1.3 Semi-Empirical Expressions

Halpin and Tsai (1967) and Halpin and Kardos (1976) used an empirical approach to obtain some generalized equations which give quite satisfactory results for unidirectional composites compared to the complicated micromechanical equations. These equations contain adjustable fitting parameters and work quite well at low fiber volume fractions. They can also provide useful estimates of properties of composites containing oriented short fibers or whiskers. The adjustable parameters must be obtained from experimental data or must conform to some analytical solution. One uses a single equation of the form:

$$\frac{p}{p_m} = \frac{1+\xi\eta V_f}{1-\eta V_f}$$

$$\eta = \frac{\frac{p_f}{p_m} - 1}{\frac{p_f}{p_m} + \xi} \qquad (6.13)$$

where p represents one of the various moduli of the composite, e.g., E_{11}, E_{22}, G_{12} or G_{23}; p_f and p_m are the corresponding matrix and fiber moduli, respectively; V_f is the fiber volume fraction; and η is a measure of reinforcement which depends on the boundary conditions (fiber geometry, fiber distribution, and loading conditions). The term ξ is a fitting parameter that is used to make Eq. (6.13) conform to the experimental data. The function ξ in Eq. (6.13) is constructed in such a way that we get the two extreme values of property corresponding to $V_f = 0$ and 1, i.e., when $V_f = 0$, we have $p = p_m$ and when $V_f = 1$, we get $p = p_f$. Furthermore, the form of η is such that:

$$p = p_f V_f + p_m V_m \quad \text{for } \xi \to \infty$$

$$1/p = V_m/p_m + V_f/p_f \quad \text{for } \xi \to 0$$

These two extremes provide the bounds, although not necessarily tight bounds, on the properties of the composite. For example, for the transverse modulus of the composite E_{ct} or E_{22}, we can write:

$$\frac{E_{ct}}{E_m} = \frac{1 + \xi\eta V_f}{1 - \eta V_f}$$

$$\eta = \frac{\frac{E_f}{E_m} - 1}{\frac{E_f}{E_m} + \xi}$$

Comparing these expressions with the exact elasticity solutions, one can obtain a value of ξ. Note that, in principle, ξ can range form 0 to ∞. ξ can be thought of as a measure of the "effectiveness" of fiber reinforcement. For small values of ξ, fibers are less effective than for large values of ξ. For computing E_{ct}, ξ = 1 or 2 works for hexagonal or square array of fibers, respectively. One can also point out some limiting values of η. The term ηV_f is akin to reduced fiber volume fraction. For a homogeneous material, η = 0. For very stiff fibers, η = 1 while for very compliant inclusions (e.g., voids) η = $-1/\xi$. Figure 6.7 shows plots of Young's modulus, E, as function of volume fraction of SiC particles in 2080 Al matrix, as per lower and upper bounds of Hashin-Shtrikman expressions, Halpin-Tsai expression, and the experimental values measured in the longitudinal and transverse directions (Ganesh and Chawla, 2005). Note that Hashin-Shtrikman and Halpin-Tsai expressions treat the composite to be an isotropic material. The experimental results show that because of particle alignment caused by extrusion, the longitudinal values of modulus are higher than the transverse values. The experimental values fall somewhere between the Hashin-Shtrikman upper and lower bounds. Figure 6.8 shows similar plots for a composite where the particles are distributed in a homogenous manner, a WC/Co composite (Koopman et al., 2002).

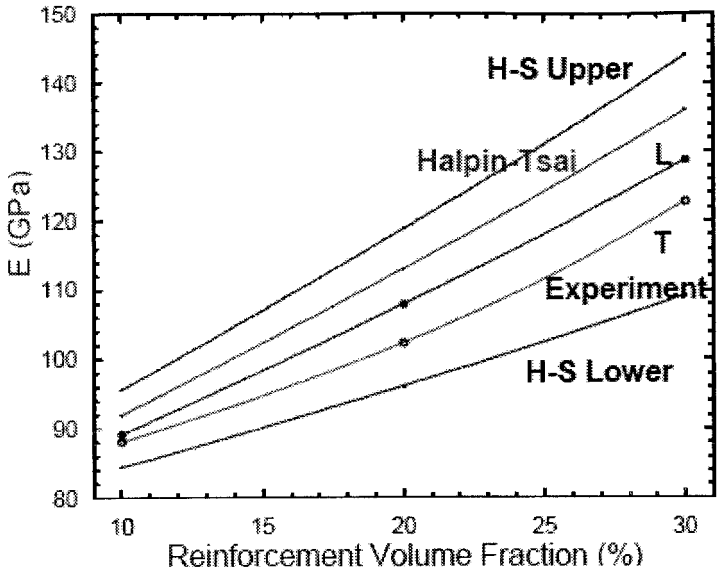

Fig. 6.7 Young's modulus, E as a function of SiC particle reinforcement showing lower and upper bounds of Hashin-Shtrikman, Halpin-Tsai expression, and the experimental values measured in the longitudinal (L) and transverse (T) directions (after Ganesh and Chawla, 2005). The experimental results show difference between longitudinal and transverse directions because of particle alignment caused by extrusion. Hashin-Shtrikman, Halpin-Tsai expressions treat the composite to be isotropic which is not quite true in this case.

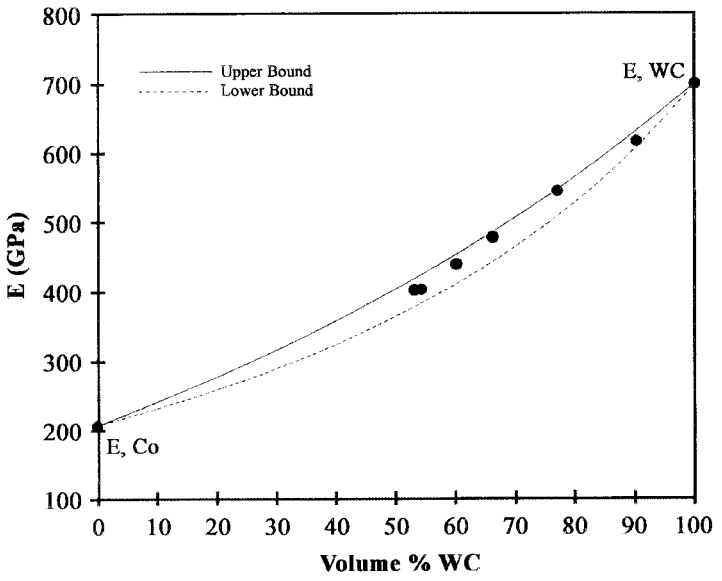

Fig. 6.8 Young's modulus, E as a function of volume fraction of WC in a WC/Co composite (after Koopman et al., 2002)

6.1.4 Eshelby Method or Equivalent Homogeneous Inclusion Technique

Eshelby (1957) formulated the problem of an elastic ellipsoidal inclusion embedded in an elastic matrix subjected to a displacement, with uniform strain field, an infinite distance away from the inclusion. The Eshelby technique provides the solution to a general problem of an infinite medium containing an inclusion. It involves replacing the real inclusion by an inclusion made of matrix (hence the use of expression *equivalent homogeneous inclusion*) but with a proper misfit strain, called *equivalent transformation strain*. The resultant stress field is the same as that for the real inclusions. In very simple terms, we can outline the technique as follows:

- Cut a piece of material from the unstressed, homogenous matrix leaving a hole.
- Allow the cut piece of material to undergo a shape change that corresponds to a transformation strain, ε^t.
- Insert the transformed inclusion back into the original hole, preventing interfacial sliding, and then releasing the tractions. This requires the application of surface tractions so that the transformed shape of the inclusion can be fit back into the original hole.

A constrained strain, ε^c is developed in the inclusion relative to the initial shape. The Eshelby tensor, S, relates the constrained strain, ε^c to the transformation strain, ε^t, by:

$$\varepsilon^c = S\varepsilon^t$$

The Eshelby tensor is a function of the aspect ratio of the inclusion (or reinforcement) and the Poisson's ratio of the matrix. The reinforcement (short fibers, whiskers, or particles) are represented as prolate spheroids. The equation for such an inclusion in terms of Cartesian coordinates is:

$$\frac{x^2 + y^2}{a^2} + \frac{z^2}{c^2} = 1$$

where c/a represents the aspect ratio of the inclusion and $c/a > 1$.

The important general result of the Eshelby analysis is that for an ellipsoidal inclusion the resulting stress and strain in the inclusion are homogeneous. The strains in the matrix and in the inclusion are therefore related

algebraically. We can write for the stress in the inclusion, σ_i, in terms of stiffness of the material, C_m, and the elastic strain in the inclusion as:

$$\sigma_i = C_m (\varepsilon^c - \varepsilon^t)$$

In a composite, the ellipsoid inclusion or reinforcement will generally be stiffer than the matrix, i.e., the reinforcement has elastic constants, C_i. The inclusion being a different material than the matrix, we need to replace ε^t with an equivalent strain. With appropriate rearrangement, the resulting stress in the inclusion is

$$\sigma_i = C_i (\varepsilon^c - \varepsilon^t_{eq})$$

Now, $\varepsilon^c \neq S\varepsilon^t_{eq}$, since $C_i \neq C_m$. However, we can find an equivalent homogenous transformation strain, ε^t, such that the equivalent inclusion resembles the inhomogeneity, i.e.:

$$C_i (\varepsilon^c - \varepsilon^t_{eq}) = C_m (\varepsilon^c - \varepsilon^t)$$

$$\text{or} \quad C_i(S\varepsilon^t - \varepsilon^t_{eq}) = C_m(S - I)\varepsilon^t \qquad (6.14)$$

From Eq. (6.14), we can obtain the transformation strain for any shape change, ε^t_{eq} and stiffness mismatch $(C_i - C_m)$ as:

$$\varepsilon^t = [(C_i - C_m)S + C_m]^{-1} C_i\varepsilon^t$$

This then gives the stress in the reinforcement as:

$$\sigma_i = C_m(S - I)[(C_i - C_m)S + C_m]^{-1} C_i\varepsilon^t \qquad (6.15)$$

This expression allows us to calculate the internal stresses in the inclusion. It is valid when the concentration of the inclusion phase is small. If this is not so, the interaction of the fields from the other inclusions would affect the average fields in the matrix and the reinforcement. The main advantage of the Eshelby tensor is that it allows us to determine the stress and strain in the inclusion without worrying about the complex stress field in the matrix. Determining the full field values can be an extremely difficult proposition depending on the geometry and the selected load case.

The Eshelby method would work nicely if the composite had ellipsoidal inclusions of arbitrary aspect ratios. The reinforcements, however, are generally of any shape causing singularities and problems in the local fields.

The averaging schemes, in general, break down for some reinforcement shapes and if there occurs a clustering of particles or fibers. Last but not least, the effect of shape and spatial distribution of particles can become quite marked when constrained plastic deformation occurs in one of the phases, for example, in a WC/Co composite.

6.1.5 Numerical Methods

As an alternative to analytical analysis, numerical techniques such as finite element method (FEM) have become very popular, especially when the geometry of the component and thermomechanical history of the composite can be incorporated into the simulation of the properties. One common approach is to use a unit-cell model, where one or more reinforcement, fibers or particles, are embedded within the matrix, to simulate a composite material with a periodic array of reinforcement. It should be noted that in actual composites the particles commonly contain sharp corners, so spherical particles are not necessarily a realistic choice for simulation. Microstructure-based finite element techniques have been employed that are able to incorporate the "true" microstructures, that take into consideration particle morphology and clustering of particles, as a basis for analysis using finite element techniques (Chawla et al., 2003, Chawla et al., 2004). Figure 6.9 shows a microstructure-based model and two unit-cell models.

Chawla et al. (2003) applied an object oriented finite element technique to particulate reinforced metal matrix composites from images (micrographs) of real systems. In particular, the effect of reinforcement particle volume fraction and alignment (with respect to the loading axis) on the anisotropy of elastic properties was investigated. Chawla et al. (2004) obtained numerical

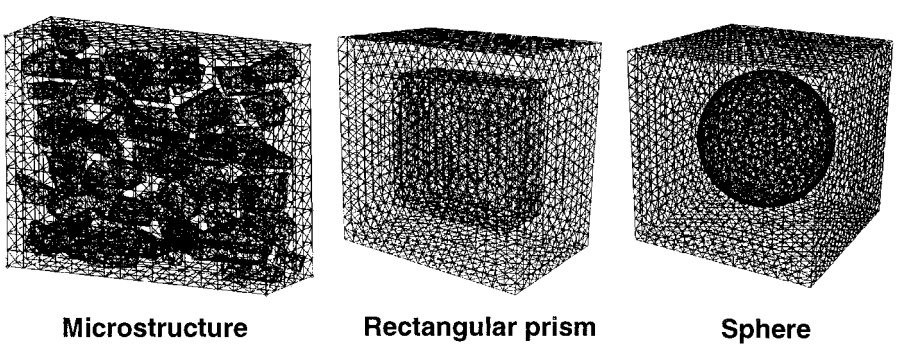

Fig. 6.9 Comparison of different types of numerical models: microstructure-based, unit cell rectangular prism, and unit cell sphere (after Chawla et al., 2004)

predictions of the effective Young's modulus for an Al/SiC_p composite, which are shown in Table 6.2. The unit cylinder particle has a greater stiffening effect than the spherical particle. Clearly, load transfer by a shear-lag type of mechanism (see chapter 7) is more effective across a planar interface than a spherical interface.

The advantage of using a three-dimensional (3D) microstructure-based model is shown by a comparison of the predicted Young's modulus of the composite, versus typical prismatic (rectangular) and spherical unit cell models, Table 6.2. The highest and lowest simulated moduli and strength were obtained by the prismatic rectangle unit cell and sphere unit cell, respectively. This can be attributed to the highest degree of load transfer for the prismatic, rectangular particle than for the spherical particles. The 3D microstructural models, from two different regions of the material, exhibited a higher degree of strengthening, since the actual microstructure incorporated the inherent aspect ratio and alignment of the SiC particles along the loading direction. A comparison of all predicted moduli with experimental tensile data on the same composite, from Chawla et al. (2004), shows that the result from the 3D microstructure model correlates very well with the experimentally determined Young's modulus value of 108 GPa (Ganesh and Chawla, 2004).

6.2 PHYSICAL PROPERTIES

In this section we provide expressions for some important physical properties such as density, coefficients of thermal expansion, and electrical and thermal conductivity.

6.2.1 Density

Density of a material is mass per unit volume. Density is one property for which the rule-of-mixtures works for any composite irrespective of the

Table 6.2 Young's Modulus Predicted by Various Finite Element Models and Comparison to Experiment (Chawla et al., 2004)

Method	Young's Modulus (GPa)
Unit Cell – Rectangular Prism	113
Unit Cell – Sphere	100
3D Microstructure	107.4 ± 0.4
Experiment (Ganesh and Chawla, 2004)	107.9 ± 0.7

distribution of the constituents. The mass of a composite is the sum of the masses of the constituents. Thus:

$$m_c = m_m + m_r \qquad (6.16)$$

where m represents the mass and the subscripts c, m, and r indicate composite, matrix, and reinforcement, respectively. The above equation is valid even in the presence of voids in the composite. For the volume of the composite, we can write:

$$v_c = v_m + v_r + v_v \qquad (6.17)$$

where v denotes the volume of a component while the subscripts c, m, r, and v indicate composite, matrix, reinforcement, and void, respectively. We can then write in terms of mass fractions and volume fractions of the composite the following two expressions:

$$M_m + M_r = 1$$

$$V_m + V_r + V_v = 1$$

For the density of the composite, we can write:

$$\rho_c = \frac{m_c}{v_c} = \frac{m_r + m_m}{v_c} = \frac{\rho_r v_r + \rho_m v_m}{v_c} = \rho_r V_r + \rho_m V_m \qquad (6.18)$$

An experimental measurement of density of a composite is frequently used to test for the presence of any porosity in the composite. It is worth pointing out that should there be any interfacial reaction between the components of a composite, the reaction product(s) should be treated as additional component(s) of the composite.

6.2.2 Coefficient of Thermal Expansion (CTE), α

Most materials, with very few exceptions, expand when heated, i.e., their volume increases. This of course stems from the atomic or molecular vibrations that materials undergo at all temperatures. The amplitude of these vibrations increases with temperature. We can characterize this in terms of a *volumetric* coefficient of thermal expansion, β, defined as:

$$\beta_{ij} = \frac{1}{V}\left(\frac{\delta V}{\delta T}\right)$$

where V is the volume of the material, T is its temperature and the two indices of the volumetric coefficient of thermal expansion indicate that it is a second rank tensor.

We can also define a *linear* coefficient of thermal expansion, α, as:

$$\alpha_{ij} = \frac{\delta \varepsilon_{ij}}{\delta T}$$

where ε is the strain and α is another second-rank symmetric tensor. The coefficient of thermal expansion, α, does not have a constant value over a very large range of temperature. Over a small temperature range, ΔT, we write:

$$\varepsilon_{ij} = \alpha_{ij}\Delta T$$

It is instructive to recall that the sum of the diagonal terms of the strain tensor represent the volume change, i.e.,

$$\beta = \varepsilon_{11} + \varepsilon_{22} + \varepsilon_{33} = 3\alpha$$

$$\alpha = \frac{1}{3}\left[\varepsilon_{11} + \varepsilon_{22} + \varepsilon_{33}\right]$$

For small strains,

$$\beta_{ij} = 3\alpha_{ij}$$

In matrix notation, we can write:

$$\begin{vmatrix} \varepsilon_{11} & \varepsilon_{12} & \varepsilon_{13} \\ & \varepsilon_{22} & \varepsilon_{23} \\ & & \varepsilon_{33} \end{vmatrix} = \begin{vmatrix} \alpha_{11} & \alpha_{12} & \alpha_{13} \\ & \alpha_{22} & \alpha_{23} \\ & & \alpha_{33} \end{vmatrix} \Delta T$$

In contracted notation, the above expression takes the following form:

$$\begin{vmatrix} \varepsilon_1 \\ \varepsilon_2 \\ \varepsilon_3 \\ \varepsilon_4 \\ \varepsilon_5 \\ \varepsilon_6 \end{vmatrix} = \begin{vmatrix} \alpha_1 \\ \alpha_2 \\ \alpha_3 \\ \alpha_4 \\ \alpha_5 \\ \alpha_6 \end{vmatrix} \Delta T$$

If we are interested in finding the CTE in any arbitrary direction [hkl] in the plane of a fiber reinforced composite, we need to use the direction cosines formula. Let α_{hkl} be the CTE along a direction [hkl] that has direction cosines n_1, n_2, and n_3.

$$\alpha_{hkl} = n_1^2\alpha_1 + (n_2^2 + n_3^2)\alpha_1$$

$$\alpha_{hkl} = \alpha_\perp \sin^2\theta + \alpha_{||} \cos^2\theta$$

$$\alpha_{hkl} = \alpha_\perp + (\alpha_{||} - \alpha_\perp) \cos^2\theta$$

where we have taken $\alpha_1 = \alpha_{||}$, parallel to the fiber axis and $\alpha_2 = \alpha_3 = \alpha_\perp$, perpendicular to the fiber axis. Also, we have made use of the relationship $n_1^2 + n_2^2 + n_3^2 = 1$. θ is the angle between direction [hkl] and the fiber axis.

Expressions for CTE of Composites

In general, the CTE of a composite is different from that given by a simple rule of mixtures ($\alpha_f V_f + \alpha_m V_m$). This is because the presence of reinforcement, with an expansion coefficient less than that of the matrix, introduces a mechanical constraint on the matrix. The degree of constraint is also dependent on the nature of the reinforcement, e.g., a fiber will cause a greater constraint on the matrix than a particle.

Many models have been proposed to predict the coefficients of thermal expansion (CTE) of fibrous and particulate composites. Experimental determination of these coefficients and analysis of the general thermal expansion characteristics of a variety of composites are available in the literature; see for example, Turner (1946); Kerner (1956); Rosen and Hashin (1970); Schapery (1968); Marom and Weinberg (1975); Vaidya and Chawla (1994).

Unidirectionally Aligned Fibrous Composites

In fiber reinforced composites, two thermal expansion coefficients are needed: α_{cl} in the longitudinal direction and α_{ct} in the transverse direction. Fibers generally have a lower expansion coefficient than that of the matrix. Thus, the fibers mechanically constrain the matrix resulting in α_{cl} being generally smaller than α_{ct} for the composite. At low V_f, it is possible that the transverse expansion coefficient of a fibrous composite, α_{ct}, may be greater than the CTE of the matrix by itself. Long, stiff fibers prevent the matrix from expanding in the longitudinal direction, which forces the matrix to expand more than usual in the transverse direction. Schapery (1968) put bounds on the coefficient of thermal expansion of a unidirectional fiber reinforced composite. These bounds are quite narrow in the longitudinal direction. The following assumptions are made in this analysis:

(a) The bonding between the fiber and matrix is perfect and mechanical in nature, i.e., no chemical interaction is allowed.
(b) The fibers are continuous and perfectly aligned.
(c) The properties of the constituents do not change with temperature.
(d) Poisson's ratios of the components are not very different.

Expressions for expansion coefficient of a fibrous composite are as follows. The longitudinal expansion coefficient for the composite is:

$$\alpha_{cl} = \frac{\alpha_m E_m V_m + \alpha_f E_f V_f}{E_m V_m + E_f V_f} \tag{6.19}$$

The transverse expansion coefficient is:

$$\alpha_{ct} \cong (1+\nu_m)\alpha_m V_m + (1+\nu_f)\alpha_f V_f - \alpha_{cl}\overline{\nu} \tag{6.20}$$

$$\overline{\nu} = \nu_f V_f + \nu_m V_m$$

For low fiber volume fractions, $V_f > 0.2$ or 0.3, α_{ct} can be approximated by

$$\alpha_{ct} \cong (1+V_m)\alpha_m V_m + \alpha_f V_f$$

Anisotropy in expansion can be reduced if the composite contains randomly oriented short fibers or whiskers in three dimensions. Fore such a composite, the isotropic thermal expansion coefficient is given by:

$$\alpha \cong \frac{\alpha_{cl} + 2\alpha_{ct}}{3}$$

Particle Reinforced Composites

One can regard a particulate composite as a homogeneous material in a statistical sense, i.e., assuming a uniform distribution of the particles in the matrix, Fig. 6.10. Volumes fractions of the two phases are:

$$V_1 \text{ and } V_2 (= 1 - V_1)$$

Volumetric CTE of a composite consisting of spherical particles dispersed in a matrix (Kerner, 1956) is given by:

$$\beta_c = \beta_m V_p + \beta_p V_p - (\beta_m - \beta_p) V_p \left[\frac{\frac{1}{K_m} - \frac{1}{K_p}}{\frac{V_m}{K_p} + \frac{V_p}{K_m} + \frac{0.75}{G_m}} \right]$$

Kerner's expression does not differ significantly from the rule of mixtures because the particle constraints the matrix a lot less than fibers. The

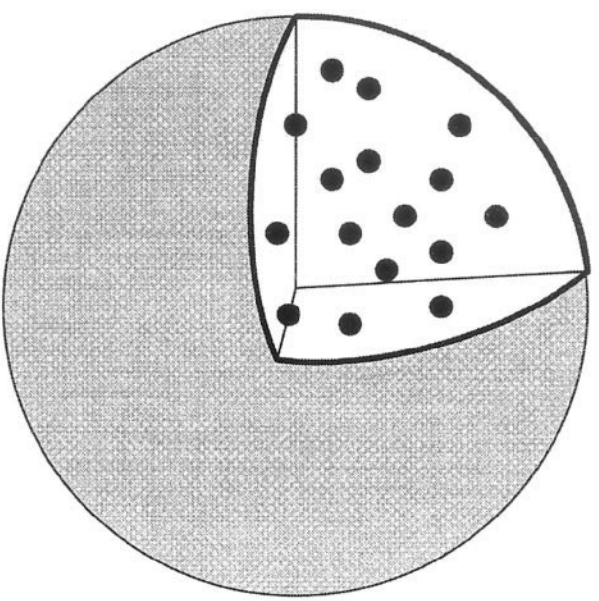

Fig. 6.10 Schematic of a particulate composite.

Schapery solution (Schapery, 1968), gives upper and lower bounds for the thermal expansion coefficient. The upper bound is given by:

$$\alpha_c = V_p\alpha_p + V_m\alpha_m + \left[\frac{4G_m}{K_c}\right]\left[\frac{(K_c - K_p)(\alpha_m - \alpha_p)V_p}{4G_m + 3K_p}\right]$$

and the lower bound is:

$$\alpha_c = V_p\alpha_p + V_m\alpha_m + \left[\frac{4G_p}{K_c}\right]\left[\frac{(K_c - K_m)(\alpha_p - \alpha_m)V_m}{4G_p + 3K_m}\right]$$

where K_c is the bulk modulus of the composite and is obtained from the Hashin-Shtrikman analytical model (Hashin and Shtrikman, 1963) described above.

The expression of the linear CTE of a particulate composite has also been given by Turner (1946):

$$\alpha_c = \frac{\alpha_m V_m K_m + \alpha_p V_p K_p}{V_p K_p + V_m K_m}$$

Turner's expression, generally, gives an expansion coefficient much lower than the rule-of-mixtures value.

The models described above have been used extensively to predict the experimental behavior of particle reinforced MMCs. Elomari et al. (1997) studied the CTE behavior of SiC particle reinforced pure Al matrix composites, in the volume fraction range of 47-55% particles. The SiC particles were oxidized prior to matrix infiltration to minimize interfacial reaction. In their study the rule-of-mixtures predicted the highest CTE, followed by the predictions of Kerner, Schapery, and Turner, which was the lowest. The experimental data were in between the broad range between Kerner and Schapery predictions. Similar trends were observed by Sadanandam et al. (1992) for composites of 2124 Al reinforced with SiC (10,20%), Al_2O_3 (20%), and TiC (20%). Vaidya and Chawla (1994) measured CTE in several particle reinforced composites, $2014/SiC/17_p$, $2014/Al_2O_3/17_p$, 8090 (Al-Li)/$SiC/15_p$, $6061/SiC/15_p$, $6061/B_4C/15_p$. Kerner's model was closest to experiment, although the Turner model predictions were much lower than the experiment. They attributed this to the fact that the Kerner's model is close to the rule of mixtures approximation

when the constraint term is small, i.e., since the reinforcement is in particulate form, the constraint is not as large as that from fiber reinforcement.

Chawla et al. (2005) studied the thermal expansion behavior of extruded SiC particle reinforced Al matrix composites, using 2D microstructures as the basis for the models, Fig. 6.11(a). The stress state in the composite was very much influenced by the morphology and distribution of the SiC particles, Fig. 6.11(b). The stress was highest at the particle/matrix interface, while the matrix between closely-spaced particles was also under high thermal stress. "Networks" of high stress regions, linking particles in the composite, were also observed. The CTE of the composites was measured in three different

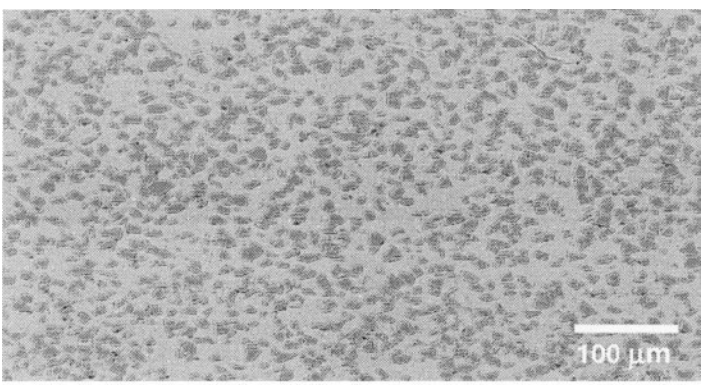

(a)

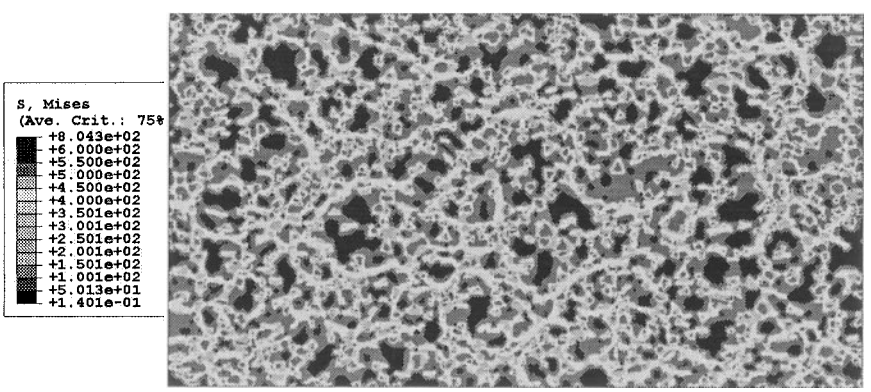

(b)

Fig. 6.11 (a) 2D microstructure used as the basis for finite element modeling of thermal expansion behavior in extruded SiC particle reinforced Al matrix composites (b) von Mises stress distribution after thermal expansion. The stress state in the composite was very much influenced by the morphology and distribution of the SiC particles (after Chawla et al., 2005).

orientations: longitudinal (parallel to the extrusion axis), transverse (normal to the extrusion axis but in the extrusion plane), and short transverse (normal to the extrusion axis, and out of the plane). They also showed that the Turner prediction was below the experimental values, while the Schapery bounds were somewhat higher than the experiments, Fig. 6.12(a). Using the microstructure-based models, better agreement was obtained with experiments than with the analytical models above. Because of the 2D nature of the model, however, the predictions were slightly higher than the experimental values, Fig. 6.12(b).

Effect of Interface on CTE of a Composite

As we have described above, most models predict a value of thermal expansion coefficient of a composite that is less than that given by a simple rule of mixtures (ROM). The CTE of the composite is generally less than the ROM value because the presence of ceramic particles (usually of low α) introduces a constraint on the expansion of the metallic matrix (usually of high α). In this regard, it is important to point out that interface can exert some influence on the value of CTE, especially for very small particle size.

Xu et al. (1994) examined the effect of particle size on the thermal expansion of Al/TiC_p composites, in which the TiC particle size was varied. In this system, the interface is semi-coherent (Mitra et al., 1993). The particle volume fraction was maintained constant at about 15% while two particle sizes were used, 0.7 μm and 4 μm. Figure 6.13 shows the values of coefficient of thermal expansion (CTE) for the two composites (circles and squares). Also plotted in Fig. 6.13 are the CTE values for pure aluminum and titanium carbide. The 4 μm particle composite showed, consistently, a higher CTE than the 0.7 μm particle composite. Note that the CTE of the 4 μm particle composite is very close to the rule of mixture (ROM) value, while that of the 0.7 μm particle composite is not, implying that more constraint on the aluminum matrix is caused by the 0.7 μm particle than by the 4.0 μm particle. A very good interfacial bond between the TiC particle and matrix exists. Although no chemical compound formation was observed in the interfacial area, lattice distortion in the interfacial area was observed. The thickness of this region of strain localization varied between 10-50 nm (Mitra et al., 1993). Such a lattice distortion at the interface will affect the CTE value of the composites. Since the interfacial area is related to the particle size, the volume of such a lattice distortion layer will depend on the particle size, and, accordingly, the effect of the particle size on the CTE of the composites will vary with the particle size as well as shape. For a given particle volume fraction, the smaller particle size, the greater the volume

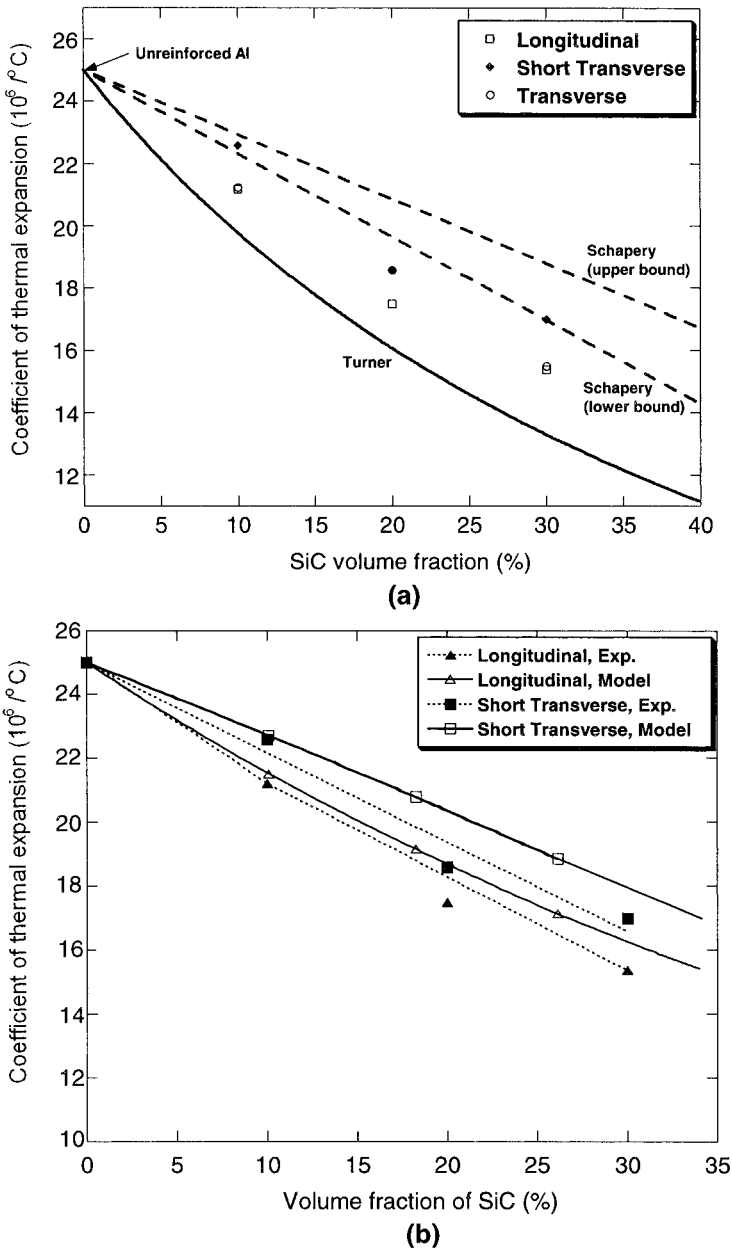

Fig. 6.12 (a) Comparison of experimentally determined CTE in extruded 2080 Al/SiC_p matrix composites, along with analytical predictions by Schapery and Turner, and (b) 2D microstructure-based FEM predictions. The effect of CTE anisotropy is more adequately captured by the microstructure-based model (after Chawla et al., 2005).

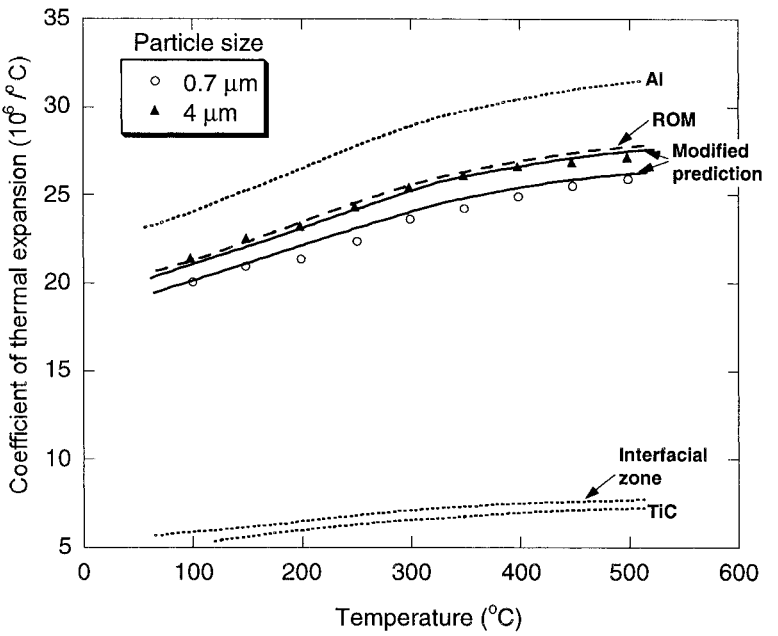

Fig. 6.13 CTE versus temperature for TiC particle reinforced Al composites with different particle size (after Xu et al., 1994). The 4 μm particle composite showed, consistently, a higher CTE than the 0.7 μm particle composite. The modified rule of mixtures (ROM) prediction, which includes the CTE of the interface, predicted the experimental behavior very well.

fraction of interfacial zone. Figure 6.14(a) illustrates the effect of particle size on the interfacial zone size for a given volume fraction of particle. A quantitative comparison of volume fraction of interfacial zone, V_i, between two particle size composites is shown in Fig 6.14(b). If the thickness of the distortion layer is assumed to be 25 nm, V_i can be 3%, which is quite significant. This interfacial zone will be constrained to expand or contract with the particle, and thus, CTE of this zone will be closer to that of the particle than that of the metal matrix. In order to explain the effect of the particle size on the CTE of the particle reinforced metal matrix composite, consider that the composite consists of a matrix phase, a particulate reinforcement, and an interfacial zone to which a CTE different from that of the matrix can be ascribed. In this approximation, the constraint on the matrix expansion is thus embedded in the interfacial zone term. We can then write for the CTE of a three-component composite as follows:

$$\alpha_c = \alpha_p V_p + \alpha_m V_m + \alpha_i V_i \qquad (6.21)$$

where the subscripts, c, p, m, and i, denote the composite, particle, matrix, and interfacial zone, respectively. The interfacial zone volume fraction, V_i, was calculated by the interfacial area and the thickness of the lattice distortion layer. The best fit CTE curves using Equation (6.21) for the 4.0 μm and 0.7 μm particle composites are obtained for the same assumed value α_i but different V_i, see the solid lines with data points in Fig. 6.13. The

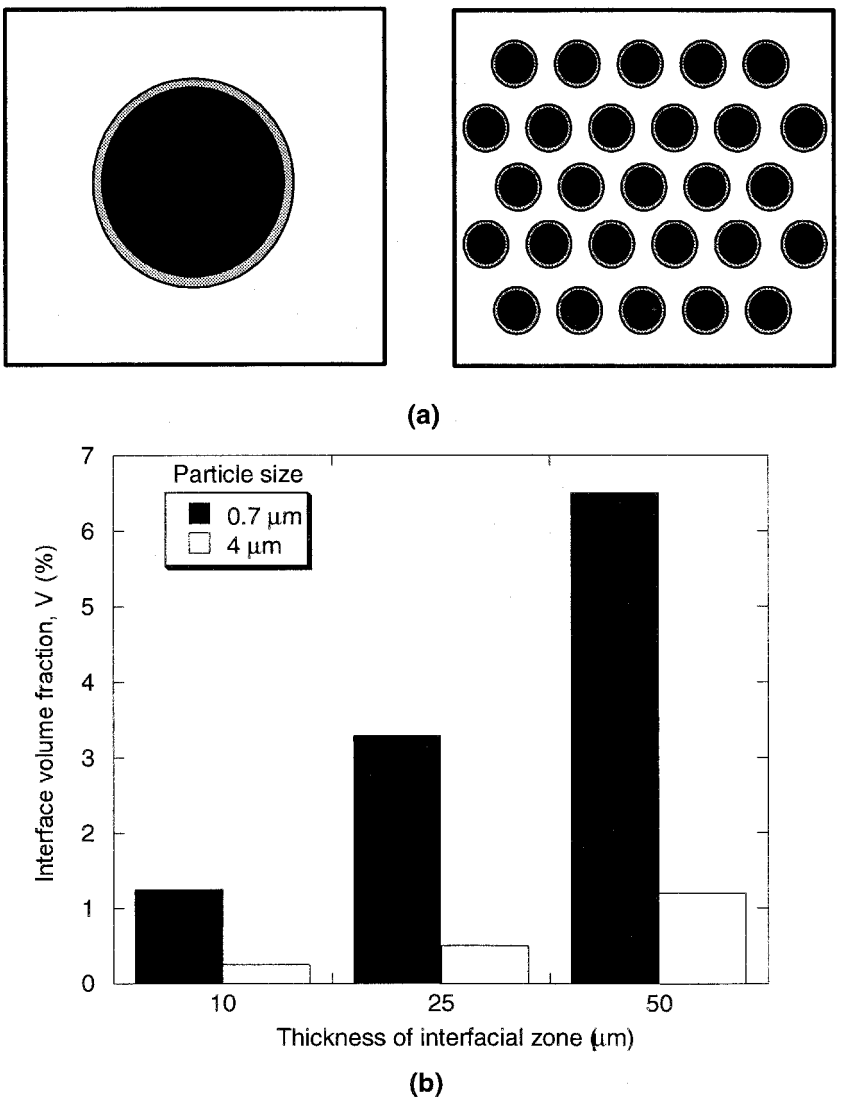

Fig. 6.14 (a) Schematic of the effect of particle size on fraction of interfacial zone. A smaller particle size results in a larger interfacial area. (b) Quantitative measurements of interfacial zone in Al/TiC_p composites. A larger interfacial zone will have a stronger effect on the CTE of the composite (after Xu et al., 1994).

apparent CTE values for the interfacial zone are also shown in Fig. 6.13. The agreement between the prediction (Eq. 6.21) and the experimental results confirms the effect of particle size on the CTE of this particle reinforced composite.

A lower CTE may also result from an interfacial phase between particle and matrix. Elomari et al. (1997) studied the CTE behavior of SiC particle reinforced pure Al matrix composites. The SiC particles were oxidized prior to matrix infiltration to minimize interfacial reaction. A thin SiO_2 coating formed on the particles resulted in a lower CTE than that of unoxidized materials. Furthermore, a decrease in particles size (i.e., more surface area for oxides to form) also resulted in reduced CTE.

Other Factors Influencing CTE of Composites

In addition to the interface, the CTE of particle reinforced MMCs is affected by several other factors. These include: Plasticity due to CTE mismatch between reinforcement and matrix, during heating or cooling; reinforcement fracture, residual stress, and local stresses at points of contact between reinforcement. Lee et al. (1991), for example, noted that the experimentally measured CTE in Al alloy/SiC_p composites was lower than that of model predictions by Paul (1960). They postulated that the irregular shape of the SiC particles may cause different thermal stress fields relative to perfectly spherical particles. Furthermore, an incompressible plastic layer may form at the particle/matrix interface, and result in lower expansion of the matrix, and thus, the overall composite.

The CTE may also be affected the particle fracture. Elomari et al. (1996) examined the CTE in particle reinforced MMCs, 6061/Al_2O_3/10_p and 20_p, with increasing particle fracture. An increase in particle fracture resulted in increased CTE. Residual stress also has an important effect on CTE. Chang et al. (2000) studied the CTE behavior of 40 vol.% Al_2O_3 particle reinforced Al matrix composites. Water-quenched simples had a lower CTE than furnace cooled simples. This was attributed to thermal residual stresses present in the water-quenched samples. At temperatures above 100°C the CTE increased, and were closer to the prediction by Kerner. This was attributed to a relief in the residual stresses with increasing temperature. Shen et al. (1994) used a unit-cell FEM approach to model the thermal expansion behavior of SiC particle reinforced Al matrix composites. They showed that residual stress increased the apparent CTE of the composite, since the residual stress in the metal matrix has a tensile component. Shen et al. (1994) also showed that the CTE is much less sensitive to particle

distribution (clustering) than tensile stiffness. This was attributed to the fact that for an elastically deforming, isotropic composite, the effective CTE is given as (per Hashin-Shtrikman and Schapery, for example):

$$\alpha = \alpha_2 + (\alpha_1 - \alpha_2)\frac{1/K - 1/K_2}{1/K_1 - 1/K_2}$$

where K is the bulk modulus and the subscripts 1 and 2 refer to ductile and brittle phases. From this equation one can see that the CTE is highly dependent on K, which is relatively insensitive to the distribution of particles in the matrix of the composite. Interestingly, the contiguity of a phase had a significant effect on CTE. For example, when the brittle phase is continuous, an additional constraint is placed on the expansion of the ductile phase. Microvoid nucleation and propagation at points where particles touch or at pre-existing processing-induced voids may also cause a deviation in strain versus temperature, with slight increase in CTE taking place (Balch et al., 1996).

6.2.3 Thermal Conductivity

Thermal conductivity is another thermal property of great importance. Some general background on thermal conductivity is given in the inset. A composite consisting of unidirectionally aligned carbon fibers in an aluminum matrix can show extremely high thermal conductivity along the fiber direction, especially if pitch-based carbon fibers are used. This is because pitch-based carbon fibers have very high thermal conductivity along the fiber axis. Thus, depending on the volume fraction of carbon fiber used, the thermal conductivity of a C/Al composite along the fiber direction can be greater than that of even copper. The thermal conductivity transverse to the fibers in such a composite will be about two-thirds that of aluminum. Such a C/Al composite can find applications in heat transfer applications where weight reduction is an important consideration. Examples of such applications might include high-density, high-speed integrated-circuit packages for computers and base plates for electronic equipment (see the chapter on applications, Chapter 11). Another possibility is to use this composite to dissipate heat from the leading edges of wings in high-speed airplanes. Tungsten carbide/cobalt composites are used extensively in operations such as metal cutting or rock drilling where they experience very high temperatures. The ability to dissipate heat away from the wear surface, and thus avoid any localized temperature-induced softening, depends on the thermal conductivity of the composite. In WC/Co composite, both phonons (quanta of lattice waves) and electrons contribute to thermal conductivity. In

ceramics, only phonon (lattice) thermal conductivity contributes to the total thermal conductivity.

The heat flow in a material is proportional to the temperature gradient, and the constant of proportionality is called the thermal conductivity. In indicial notation, the equation for heat transfer is

$$q_i = -k_{ij}\, dT/dx_j$$

where q_i is the heat flux along x_i axis, dT/dx_j is the temperature gradient across a surface that is perpendicular to the x_j axis, and the coefficient, k_{ij} is called thermal conductivity. Thermal conductivity is also a second-rank tensor, note the two indexes. Similar to thermal expansion coefficient, the second rank, symmetric thermal conductivity tensor, k_{ij}, in an isotropic material reduces to a scalar number, k. In an orthotropic material, we need three constants along the three principal axes: k_{11}, k_{22}, and k_{33}. In a transversely isotropic material such as a unidirectionally reinforced fibrous composite, there will be two constants: k_{cl}, in the axial direction and k_{ct} in the transverse direction. The thermal conductivity in the axial direction, k_{cl} can be predicted by a rule-of-mixtures type expression (Behrens, 1968)

$$k_1 = k_{cl} = k_{fl} V_f + k_m V_m$$

where k_{fl} is the thermal conductivity of the fiber in the axial direction and k_m is the thermal conductivity of the isotropic matrix. This relationship is similar to the rule-of-mixtures in the longitudinal direction for the Young's modulus obtained by action-in-parallel.

Thermal conductivity of a unidirectionally aligned fiber composite (i.e., transversely isotropic) in the transverse direction can be approximated by the action-in-series model. This would give:

$$k_{ct} = k_2 = k_{f2}\, k_m/(k_{f2} V_f + k_m V_m)$$

Halpin-Tsai-Kardos equations can be used to obtain the following expression for the transverse thermal conductivity of a composite containing unidirectionally aligned fibers:

$$k_{c2} = k_{c3} = k = (1 + \eta V_f)/(1 - \eta V_f) k_m$$
$$\text{and } \eta = [(k_{f2}/k_m) - 1]/[(k_{f2}/k_{fm}) + 1]$$

Transport Properties

Electrical and thermal conductivities represent two very important transport properties. Electrical resistivity, ρ, is the inverse of electrical conductivity, σ. Electrical resistance of a piece of metal of length, L, and cross-sectional area, A, is given by:

$$R = \frac{L\rho}{A}$$

Ohm's law relates the voltage drop, V and current, I as V= IR. Another form of Ohm's laws is as follows:

$$J_i = \sigma_{ij} E_j \qquad (A)$$

where J is the current density (current per unit area) I/A (Am^{-2}), E is the electric field (Vm^{-1}), and σ is the electrical conductivity ($\Omega^{-1}m^{-1}$), which is equal to 1/ρ. Metals are generally good conductors with σ on the order of 10^7 $\Omega^{-1}m^{-1}$. In general, impurities, solid solution alloying, plastic deformation reduce the electrical conductivity of metals.

The heat flow in a material is proportional to the temperature gradient, and the constant of proportionality is called the thermal conductivity. The basic equation has the form:

$$q_i = -k_{ij}\, dT/dx_j$$

where q_i is the heat flux along x_i axis, dT/dx_j is the temperature gradient across a surface that is perpendicular to the x_j axis, and k_{ij} is the thermal conductivity. Thermal conductivity is also second-rank tensor, note the two indexes. Another form of heat transfer equation is

$$q_i = -k_{ij}\, \Delta T \qquad (B)$$

where q_i is the heat flux, ΔT is the temperature gradient and k_{ij} the thermal conductivity tensor (W/mK). Equations A and B are mathematically similar. In these equations, the quantity on the left hand side is the response to the stimulus on the right hand side. The two are related via a constant of proportionality (σ and k) which is a tensor of rank two. For cubic symmetry, the tensor reduces to a scalar.

where we have taken ξ equal to 1.

For a unidirectionally reinforced fibrous composite, if we know the thermal conductivity in directions 1 and 2, we can find the thermal conductivity k_x and k_y in any arbitrary directions, x and y, respectively, by the following equations:

$$k_x = k_1 \cos^2\theta + k_2 \sin^2\theta$$

$$k_y = k_1 \sin^2\theta + k_2 \cos^2\theta$$

$$k_{xy} = (k_2 - k_1) \sin\theta \cos\theta$$

where θ is the angle measured from the x-axis to the 1-axis and k_{xy} can be considered to be a thermal coupling coefficient.

6.2.4 Electrical Conductivity

In terms of electrical conductivity, most metal matrix composites are mixtures of good electrical conductors (e.g., Cu, Al, Ti, etc.) and insulators (e.g., B, C, SiC, Al_2O_3, etc.). There are exceptions such as W/Cu composites. Some general background on electrical conductivity is given in the inset. The conductivity (thermal or electrical) of a composite will depend on the conductivity characteristics of the matrix, reinforcement, volume fraction and aspect ratio and shape of the reinforcement, and, of course, the interfacial characteristics (Weber et al., 2003a, 2003b; Weber, 2005). In particular, interfacial resistance will vary with the form and size of reinforcement and the connectivity of the phases. Weber (2005) analyzed the influence of reinforcement size on the electrical conductivity of a metal matrix composite. He explained the observed size effect in terms of additional scattering of the conduction electrons at the metal/ceramic particle interface. The scattering effect of dislocations, generated by plastic deformation in the metal matrix during cooling from the processing temperature, on electrical conductivity was not significant.

For the simple case of a fiber reinforced composite, assuming no significant interfacial effect, we can write for the resistivity of the composite in the axial direction, in a manner similar to other rule-of-mixtures type relationships,

$$\rho_{c\ell} = \rho_1 V_1 + \rho_2 V_2$$

where ρ is the electrical resistivity, V is volume fraction of a phase, and the subscripts cℓ, 1, and 2 designate the composite in the longitudinal direction and the two components of the composite, respectively. Or in terms of electrical conductivity, σ (unfortunately, it is customary to use the same symbol as that for strength), we can write:

$$\sigma_{c\ell} = \sigma_1 V_1 + \sigma_2 V_2$$

In the transverse direction, we have:

$$\frac{1}{\sigma_{ct}} = \frac{V_1}{\sigma_1} + \frac{V_2}{\sigma_2}$$

where the symbols have the significance given earlier. There is a logarithmic expression also:

$$\log \sigma_c = V_1 \log\sigma_1 + V_2 \log\sigma_2$$

Of course, one can generalize these expressions to more than two composites in the composite, should that be the case. One can also use self-consistent models to obtain the electrical conductivity of a composite, see for example, Hale (1976).

An important point that needs to be emphasized here is that the electrical resistivity (and therefore electrical conductivity) of the metal matrix in a composite is likely to be different from that of the unreinforced metal. This is because of possible plastic deformation during processing which will introduce dislocations due to thermal mismatch between the matrix and the reinforcement. The dislocations in turn will increase the resistivity of the matrix. Unlike the unreinforced metal, one cannot recover electrical conductivity by resorting to an annealing treatment because the annealing treatment will again cause plastic deformation of the matrix because of the thermal mismatch between the components.

6.3 THERMAL STRESSES IN COMPOSITES

Thermal stresses are internal stresses that arise when a constraint on free dimensional change of a body exists (Chawla, 1973a, 1973b). In the absence of this constraint, the body can experience free thermal strains without any accompanying thermal stresses. In a composite material, this constraint comes from the fact that it is made of dissimilar materials, i.e., materials having different coefficients of thermal expansion. Thermal stresses result

in a composite because of the ever present mismatch in the coefficients of thermal expansion of the reinforcement and the matrix ($\Delta\alpha = \alpha_r - \alpha_m$). Thermal strain, in the absence of any temperature gradients, is given by $\Delta\alpha\Delta T$, where ΔT is the amplitude of temperature change. During cooling from the processing temperatures, a large magnitude of thermal stresses can result because of the thermal mismatch between the reinforcement (particle, short fiber or long fiber) and the matrix. Thermal stresses generated will depend on the reinforcement volume fraction, reinforcement geometry, thermal mismatch, temperature interval ($T_{final} - T_{initial}$), and modulus ratio, E_r/E_m, where the subscript r denotes the reinforcement. Generally, $\alpha_m > \alpha_r$, i.e., on cooling from $T_{initial}$ to T_{final} ($T_{initial} > T_{final}$), the matrix would tend to contract more than the reinforcement, putting the reinforcement in compression and the matrix in tension. That is the explanation in simple terms. In reality, it is complex three-dimensional situation. We derive below the analytical expressions for (three-dimensional) thermal stress components in two types of composites: a central particle surrounded by its associated spherical matrix shell and a central fiber surrounded by its cylindrical shell of matrix. The following assumptions are made in this analysis:

- Matrix and reinforcement obey Hooke's law.
- Elastic reinforcement is embedded in an elastic continuum of matrix.
- No chemical reactions between reinforcement and matrix.

In what follows, we need to use the following sets of relationships to solve problems in elasticity involving a complex state of stress:

- Equations of equilibrium of forces
- Equations of compatibility
- Constitutive equations (stress-strain relations)
- Boundary conditions

6.3.1 Thermal Stresses in Particulate Composites

Consider a particulate composite consisting of small ceramic particles distributed in a ceramic matrix. If we regard this composite as an assembly of elastic spheres of uniform size embedded in an infinite elastic continuum, then it can be shown from the theory of elasticity (Timoshenko and Goodier, 1951; Brooksbank and Andrews, 1970) that an axially symmetrical stress distribution will result around each particle. Figure 6.15 shows a schematic of such a particle reinforced composite. Let us say that each particle has a radius, a while the surrounding matrix sphere has the outer radius, b. This spherical symmetry problem calls for the use of spherical coordinates, r, θ,

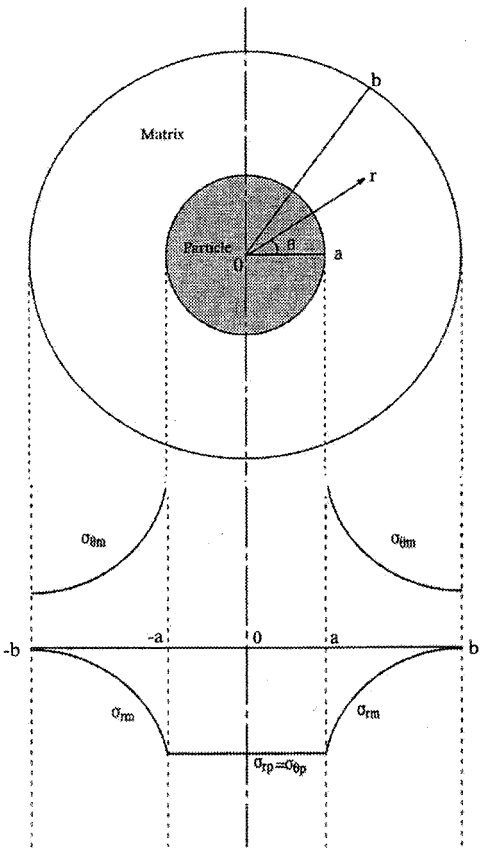

Fig. 6.15 Thermal stress distribution, on cooling, in a particulate composite that has CTE of matrix, α_m > particle CTE, α_p. The particle is under a uniform pressure, P, while the matrix has radial and tangential stress components, radial and tangential components in the matrix vary with distance as $1/r^3$.

and φ as indicated in Fig. 6.15. We have the following stress, strain, and displacement components:

$$\sigma_r,\ \sigma_\theta = \sigma_\varphi$$

$$\varepsilon_r,\ \varepsilon_\theta = \varepsilon_\varphi$$

$$u_r = u, \text{ independent of } \theta \text{ or } \varphi$$

The stress-strain and strain-displacement relationships are:

$$\varepsilon_\theta = \frac{u}{r} = \frac{1}{E}[\sigma_\theta(1-\upsilon) - \upsilon\sigma_r] + \alpha\Delta T = \varepsilon_\varphi$$
$$\varepsilon_r = \frac{du}{dr} = \frac{1}{E}[\sigma_r(1-\upsilon) - \upsilon\sigma_\theta] + \alpha\Delta T \qquad (6.22)$$

The equilibrium equation for this spherical problem is

$$\frac{d\sigma_r}{dr} + \frac{2(\sigma_r - \sigma_\theta)}{r} = 0 \qquad (6.23)$$

From Eqs. (6.22) and (6.23), we get the following governing differential equation:

$$\frac{d^2u}{dr^2} + \frac{2}{r}\frac{du}{dr} - \frac{2}{r^2}u = 0 \qquad (6.24)$$

The solution to this differential equation is:

$$u = Ar + \frac{C}{r^2} \qquad (6.25)$$

This is the general solution that gives the displacement as a function of radial distance. We can obtain our stress components by applying the following boundary conditions relevant to our problem:

(i) stress vanishes at the free surface (i.e., at r = b)

(ii) the radial stress at the interface (r = a) is the interfacial pressure, P, i.e., $\sigma_r(a) = -P$.

When we apply these boundary conditions, we find that the stresses in the particle are:

$$\sigma_{rp} = \sigma_{\theta p} = -P$$

while the stresses in the matrix are:

$$\sigma_{rm} = \frac{P}{1-V_p}\left[\frac{a^3}{r^3} - V_p\right] \text{ and } \sigma_{\theta m} = -\frac{P}{1-V_p}\left[\frac{1}{2}\frac{a^3}{r^3} + V_p\right]$$

The expression for P becomes:

$$P = \frac{(\alpha_m - \alpha_p)\Delta T}{\left[\frac{0.5(1+\nu_m)+(1-2\nu_m)V_p}{E_m(1-V_p)} + \frac{1-2\nu_p}{E_p}\right]} \qquad (6.26)$$

$$V_p = \left(\frac{a}{b}\right)^3$$

In the above expressions, V_p is the particle volume fraction, a is the particle radius, b is the matrix outer radius, and other symbols have the significance given earlier. A schematic of the stress distribution in the particulate composite is shown in the bottom half of Fig. 6.15 for case of cooling for a particulate composite that has CTE of matrix, α_m > particle CTE, α_p. We can summarize the main results for a particulate composite as follows:

- The particle is under a uniform pressure, P.
- The matrix has radial and tangential stress components that vary as $1/r^3$.
- The radial component goes to zero at the free surface, r = b, as per our boundary conditions. The tangential component has a nonzero value at the free surface.

6.3.2 Thermal Stresses in Fiber Reinforced Composites

This important problem has been analyzed by a number of researchers (Poritsky, 1934; Hull and Berger, 1934; Chawla and Metzger, 1972; Scherer, 1986; Herrmann and Wang, 1991; Hsueh et al., 1988). In the case of a unidirectionally reinforced fibrous composite, it is convenient to use polar coordinates because of the inherent cylindrical symmetry. Figure 6.16 shows the basic fiber/matrix unit consisting of a central fiber (radius, a) surrounded by its sleeve of matrix (outer radius, b). The matrix outer radius, b, will depend on the volume fraction of the matrix. Such a simple axisymmetric model can be used to obtain the three-dimensional state of thermal stress up to a moderate fiber volume fraction.

The axial symmetry means that we can treat the problem in terms of the principal stresses that are independent of θ. We derive expressions for the thermal stresses in a two-element cylindrical composite. For the axial

symmetric case under consideration, the radial and circumferential stresses will have expressions of the following form (Poritsky, 1934; Hull and Berger, 1934; Chawla and Metzger, 1972):

$$\varepsilon_r = \frac{\partial u}{\partial r} = \frac{1}{E}\left[\sigma_r - \upsilon\left(\sigma_\theta + \sigma_2\right)\right] + \alpha\Delta T$$

$$\varepsilon_\theta = \frac{u}{r} = \frac{1}{E}\left[\sigma_\theta\left(1-\upsilon\right) - \upsilon\left(\sigma_1 + \sigma_2\right)\right] + \alpha\Delta T \qquad (6.27)$$

$$\varepsilon_z = \frac{\partial w}{\partial z} = \frac{1}{E}\left[\sigma_z - \upsilon\left(\sigma_r - \sigma_\theta\right)\right] + \alpha\Delta T$$

The only equilibrium equation for this rotationally symmetric problem is:

$$\frac{d\sigma_r}{dr} + \frac{\left(\sigma_r - \sigma_\theta\right)}{r} = 0 \qquad (6.28)$$

From Eqs. (6.27) and (6.28), we get the governing differential equation for our problem:

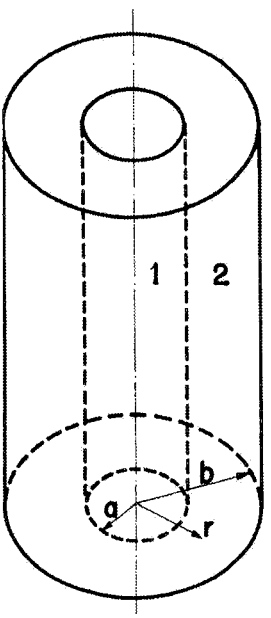

$$\frac{d^2u}{dr^2}+\frac{1}{r}\frac{du}{dr}-\frac{u}{r^2}=0 \qquad (6.29)$$

The general solution to this differential equation is:

$$u = Ar+\frac{C}{r} \qquad (6.30)$$

This relationship between displacement, u and radial distance, r needs to be solved for each component, central fiber and outer matrix sleeve by applying boundary conditions. Thus, in component 1 or fiber, we have:

$$u_1 = A_1r+\frac{C_1}{r} \qquad (6.31)$$

and in component 2 or matrix, we have:

$$u_2 = A_2r+\frac{C_2}{r} \qquad (6.32)$$

The constants of integrations in these expressions need to be obtained by applying our boundary conditions. The boundary conditions are:

(i) Stress vanishes at the free surface, i.e., $\sigma_{r2} = 0$ at $r = b$.
(ii) Continuity of displacement at the fiber/matrix interface, i.e., $u_1 = u_2$ at $r = a$.
(iii) Continuity of radial stress at the fiber/matrix interface, i.e., $\sigma_{r1} = \sigma_{r2}$ at $r = a$.
(iv) The radial displacement, u must vanish at the axis of symmetry, i.e., $u_1 = 0$ at $r = 0$.

By using these boundary conditions, we can determine the constant of integration in Eqs. (6.31) and (6.32). The last condition gives C_2 to be identically zero because if that were not so, u_1 will become infinity at $r = 0$. That leaves us with three equations and three unknowns. Since ceramic fibers used to reinforce metals remain elastic until fracture but the metal can undergo plastic deformation in response to the thermal stresses generated, we give below full expressions for the three stress components in the matrix. These are:

$$\sigma_r = A\left(1-\frac{b^2}{r^2}\right) \quad \sigma_\theta = A\left(1+\frac{b^2}{r^2}\right) \quad \sigma_z = B \qquad (6.33)$$

where we have omitted the subscript m, and the constants A and B have the following expressions:

$$A = -\left(\frac{E_m(\alpha_m - \alpha_f)\Delta T(a/b)^2}{1+(a/b)^2(1-2)[(b/a)^2-1](E_m/E_f)}\right)$$

$$B = \frac{A}{(a/b)^2}\left(2\nu\left(\frac{a}{b}\right)^2 \frac{1+(a/b)^2(1-2\nu\nu+(a/b)^2(1-2\nu)[(b/a)^2-1](E_m/E_f)}{1+[(b/a)^2-1](E_m/E_f)}\right)$$

$$\text{and } \nu_m = \nu_f = \nu$$

This thermoelastic solution can provide information about the magnitude of the elastic stresses involved and if the elastic range will be exceeded or not. In the case of a metallic matrix, it is likely to deform plastically in response to these thermal stresses (Chawla, 1973a; Chawla, 1973b; Arsenault and Fisher, 1983; Christman and Suresh, 1988). We can draw some important conclusions from Figure 6.17:

(i) Axial stress is uniform in fiber and matrix, although its magnitude is different in the two and depends on the respective elastic constants.

(ii) In the fiber, i.e., the central component f, σ_{rf} and $\sigma_{\theta f}$ are equal in magnitude and sense. In the matrix, i.e., the sleeve, σ_{rm} and $\sigma_{\theta m}$ vary as [1 – (b5/r5)] and [1 + (b5/r5)], respectively.

(iii) When either the temperature difference or the expansion coefficient difference goes to zero, the thermal stresses vanish, as expected.

As an illustration, the variation of thermal stresses generated in the magnesium matrix in an alumina fiber/magnesium matrix as a function of radial distance from the interface is plotted in Fig. 6.18. The stress values correspond a cooling of $-1^\circ C$. Normalized radial distance is used, i.e., r/a = 1 corresponds to the interface. Note the constant value of the axial stress. Also to be noted is the compressive radial stress, which is highest at the fiber/matrix interface and goes to zero at the free surface. The tangential stress is tensile in nature, highest at the interface and drops to a positive value at the surface.

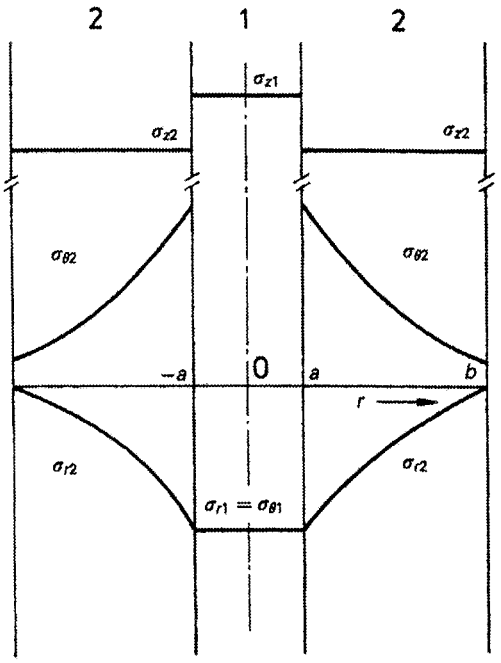

Fig. 6.17 Schematic of three-dimensional stress distribution in a fiber reinforced composite. 1 and 2 indicate fiber and matrix, respectively.

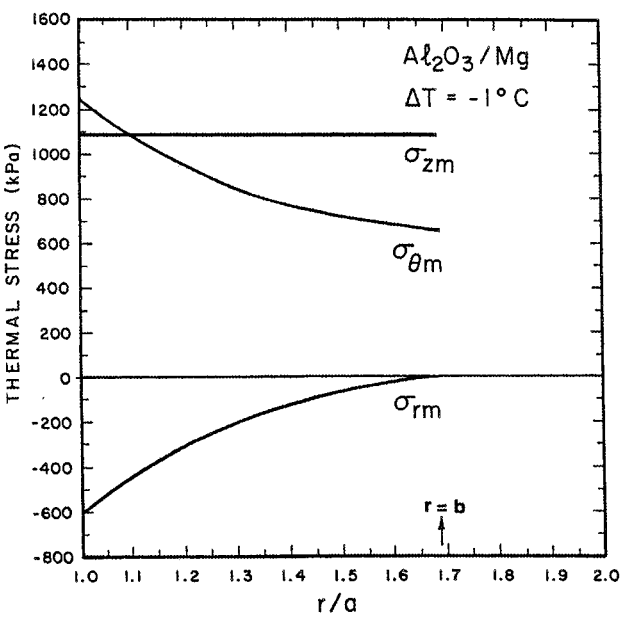

Fig. 6.18 Thermal stress distribution in magnesium matrix in an alumina fiber/magnesium matrix composite as a function of radial distance from the interface. The stress values correspond a cooling of $-1°C$. Normalized radial distance is used, i.e., r/a = 1 corresponds to the interface.

References

Arsenault, R.J., and R.M. Fisher, (1983) *Scripta Metall.*, **17,** 67.

Balch, D.K., T.J. Fitzgerald, V.J. Michaud, A. Mortensen, Y.-L. Shen, and S. Suresh, (1996) *Metall. Mater. Trans.*, **27A**, 3700-3717.

Behrens, E., (1968) *J. Composite Mater.*, **2**, 2.

Brooksbank, D., and K.W Andrews, (1970) *J. Iron and Steel Inst.*, **208,** 582.

Chang, S.-Y., S.-J. Lin, and M.C. Flemings, (2000) *Metall. Mater. Trans.*, **31A**, 291-298.

Chawla, K.K., (1973a) *Phil. Mag.*, **28**, 401.

Chawla, K.K., (1973b) *Metallography*, **6**, 55.

Chawla, K.K., and M. Metzger, (1972) *J. Mater. Sci.*, **7,** 34.

Chawla, N., B.V. Patel, M. Koopman, K.K. Chawla, R. Saha, B.R. Patterson, E.R. Fuller, and S.A. Langer, (2003) *Mater. Charac.*, **49,** 395-407.

Chawla, N., V.V. Ganesh, and B. Wunsch, (2004) *Scripta Mater.*, **51,** 161-165.

Chawla, N., X. Deng, and D.R.M. Schnell, (2005) *Mater. Sci. Eng.*, submitted.

Christman, T., and S. Suresh, (1988) *Acta Metall.*, **36**, 1691.

Elomari, S., R. Boukhili, and D.J. Lloyd, (1996) *Acta Mater.*, **44**, 1873-1882.

Elomari, S., R. Boukhili, C. San Marchi, A. Mortensen, and D.J. Lloyd, (1997) *J. Mater. Sci.*, **32**, 2131-2140.

Eshelby, J. D., (1957) *Proc. Royal Soc.*, **A241**, 376-396.

Ganesh, V.V., and N. Chawla, (2004) *Metall. Mater. Trans.*, **35A**, 53-62.

Ganesh, V.V., and N. Chawla, (2005) *Mater. Sci. Eng.*, **A391**, 342-353.

Hale, D. K., (1976) *J. Mater. Sci.*, **11**, 2105.

Halpin, J.C., and J.L. Kardos, (1976) *Polymer Eng. Sci.*, **16**, 344.

Halpin, J.C., and S.W. Tsai, (1967) "Environmental Factors Estimation in Composite Materials Design," AFML TR 67-423.

Hermans, J.J., (1967) *Proc. K. Ned.Akad. Wet.*, **B70** (1), 1.

Herrman, K.P., and Y.Q. Wang, (1991) in *Inelastic Deformation of Composite Materials*, Springer-Verlag, New York, p. 445.

Hashin, Z., (1962) *J. Appl. Mech.*, **29**, 143-53.

Hashin Z., and B.W. Rosen, (1964) *J. Appl. Mech.*, **31**, 233.

Hashin, Z., and S. Shtrikman, (1963) *J. Mech. Phys. Solids*, **11**, 127-140.

Hill, R., (1964) *J. Mech. Phys. Solids*, **12**, 199.

Hill, R., (1965) *J. Mech. Phys. Solids*, **13**, 189.

Hsueh, C.-H., P.F. Becker, and P. Angelini, (1988) *J. Am. Ceram. Soc.*, **71**, 929-933.

Hull, A.W., and E.E. Burger, (1934) *Physics*, **5**, 384.

Kerner, E.H., (1956) *Proc. Phys. Soc.*, **B69**, 808.

Koopman, M., K.K. Chawla, C. Coffin, B.R. Patterson, X. Deng, B.V. Patel, Z. Fang, and G. Lockwood, (2002) *Adv. Eng. Mater.*, **4**, 37.
Lee, Y.S., M.N. Gungor, T.J. Batt, and P.K. Liaw, (1991) *Mater. Sci. Eng.*, **A145**, 37-46.
Marom, G.D., and A. Weinberg, (1975) *J. Mater. Sci.*, **10**, 1005.
Mitra, R., W.A. Chiou, M.E. Fine, and J.R. Weertman, (1993) *J. Mater. Res.*, **8**, 2300.
McDanels, D.L., R.W. Jech, and J.W. Weeton, (1965) *Trans. TMS-AIME*, **233**, 636.
Paul, B., (1960) *Trans. AIME*, **218**, 36.
Poritsky, H., (1934) *Physics*, **5**, 406.
Rosen, B.W., (1973) *Composites*, **4**, 16.
Rosen, B.W., and Z. Hashin, (1970) *Int. J. Eng. Sci.*, **8,** 15.
Rossoll, A., B. Moser, and A. Mortensen, (2005) *Mech. Mater.*, **37**, 1.
Sadanandam, J., G. Bhikshamaiah, B. Gopalakrishna, S.V. Suryanarayana, Y.R. Mahajan, and M.K. Jain, (1992) *J. Mater. Sci. Lett.*, **11**, 1518-1520.
Schapery, R.A., (1968) *J. Comp. Mater.*, **2**, 380.
Scherer, G., (1986) *Relaxation in Glass and Composites*, Wiley, New York.
Shen, Y.-L., A. Needleman, and S. Suresh, (1994) *Metall. Mater. Trans.*, **25A**, 839-850.
Timoshenko, S., and J.N. Goodier, (1951) *Theory of Elasticity*, McGraw-Hill, New York, p. 416.
Turner, P.S., (1946) *J. Res. Natl. Bur. Stand.*, **37**, 239.
Vaidya, R.U., and K.K. Chawla, (1994) *Composites Sci. Tech.*, **50**, 13.
Weber, L., (2005) *Acta Mater,* **53**, 1945.
Weber, L., J. Dorn, and A. Mortensen, (2003a) *Acta Mater.*, **51**, 3199
Weber, L., C. Fischer, and A. Mortensen, (2003b) *Acta Mater.*, **51**, 495.
Xu, Z.R., K.K. Chawla, R. Mitra, and M.E. Fine, (1994) *Scripta Metall. Mater.*, **31**, 1525.
Whitney, J.M., and M.B. Riley, (1966) *AIAA Journal*, **4**, 1537.